

IMPROVEMENT OF RADAR DETECTION
BY DOPPLER PATTERN MATCHING

A THESIS SUBMITTED TO
THE GRADUATE SCHOOL OF NATURAL AND APPLIED SCIENCES
OF
MIDDLE EAST TECHNICAL UNIVERSITY

BY

DUYGU ÇELEBİ

IN PARTIAL FULFILLMENT OF THE REQUIREMENTS
FOR
THE DEGREE OF MASTER OF SCIENCE
IN
ELECTRICAL AND ELECTRONICS ENGINEERING

SEPTEMBER 2006

Approval of the Graduate School of Natural and Applied Sciences

Prof. Dr. Canan ÖZGEN

Director

I certify that this thesis satisfies all the requirements as a thesis for the degree of Master of Science.

Prof. Dr. İsmet ERKMEN

Head of Department

This is to certify that we have read this thesis and that in our opinion it is fully adequate, in scope and quality, as a thesis for the degree of Master of Science.

Prof. Dr. Mete SEVERCAN

Supervisor

Examining Committee Members

Prof. Dr. Yalçın TANIK (METU, EE)

Prof. Dr. Mete SEVERCAN (METU, EE)

Assoc. Prof. Dr. Sencer KOÇ (METU, EE)

Assist. Prof. Dr. Ali Özgür YILMAZ (METU, EE)

Ülkü DOYURAN (ASELSAN)

I hereby declare that all information in this document has been obtained and presented in accordance with academic rules and ethical conduct. I also declare that, as required by these rules and conduct, I have fully cited and referenced all material and results that are not original to this work.

Name, Last name: Duygu Çelebi

Signature :

ABSTRACT

IMPROVEMENT OF RADAR DETECTION BY DOPPLER PATTERN MATCHING

ÇELEBİ, Duygu

M.Sc., Department of Electrical and Electronics Engineering

Supervisor: Prof. Dr. Mete SEVERCAN

September 2006, 86 pages

In this thesis, improvement of Cell Averaging Constant False Alarm Rate (CA CFAR) radar processors is studied. A new improvement method is proposed that will reduce probability of false alarm while keeping probability of detection at good values. This method makes use of Doppler spreading patterns that appear after Doppler processing. Therefore this method is called Doppler Pattern Matching (DPM).

Performance of the algorithm has been investigated by Monte Carlo simulations. In order to evaluate the performance, improvement factor is calculated which is the ratio of the probability of false alarm of original detector to the false alarm of improved detector. It is observed that improvement factor changes depending on the simulation scenario. Almost in every case, good improvement factor can be obtained. Moreover, in most of the cases, there has been no reduction in probability of detection after DPM is applied to CA CFAR detector.

Keywords: CA CFAR, Doppler pattern matching

ÖZ

RADAR TESPİTİNİN DOPPLER ÖRÜNTÜ EŞLEMESİ YOLUYLA İYİLEŞTİRİLMESİ

ÇELEBİ, Duygu

Yüksek Lisans, Elektrik ve Elektronik Mühendisliği Bölümü

Tez Yöneticisi: Prof. Dr. Mete SEVERCAN

Eylül 2006, 86 sayfa

Bu tezde Hücre Ortalamalı Sabit Yanlış Alarm Oranı (CA CFAR) radar işlemcilerinin iyileştirilmesi incelenmiştir. Yanlış alarm olasılığını düşüren ve aynı zamanda tespit olasılığını iyi seviyelerde tutan bir iyileştirme metodu önerilmiştir. Bu metot, Doppler işleme sonrasında gözlenen Doppler'de yayılma örüntülerinden faydalanmaktadır. Bu yüzden bu metoda Doppler Örüntü İşleme(DPM) denmiştir.

Algoritmanın performansı Monte-Carlo bilgisayar benzetimleriyle incelenmiştir. Performansı değerlendirmek için iyileştirme faktörü hesaplanmıştır. İyileştirme faktörü, iyileştirme öncesi yanlış alarm olasılığının iyileştirme sonrası yanlış alarm olasılığına oranıdır. İyileştirme oranının bilgisayar benzetimlerinde kullanılan senaryoya göre değiştiği gözlenmiştir. Birçok durumda, iyi bir iyileştirme oranı elde edilmiştir. Bundan başka, DPM uygulandıktan sonra hemen hemen her durumda tespit olasılığında bir düşüş olmamıştır.

Anahtar kelimeler: CA CFAR, Doppler örüntü eşlemesi

To my family

ACKNOWLEDGEMENTS

I wish to express my sincere gratitude to my advisor Prof. Dr. Mete Severcan for his supervision, valuable guidance and helpful suggestions.

I am also grateful to ASELSAN Inc. for facilities provided for the completion of this thesis.

I would like to thank to Ülkü Doyuran for her continuous support during this study.

Special thanks to my friends Hande Doğan, Mehmet Köseoğlu and Mehmet Sami Ezercan for their helps about writing this thesis.

Special appreciation and gratitude are also due to my family for their encouragement, reassurance, endless love and understanding of spending lots of time on this thesis.

TABLE OF CONTENTS

PLAGIARISM.....	iii
ABSTRACT	iv
ÖZ.....	v
ACKNOWLEDGEMENTS.....	vii
TABLE OF CONTENTS	viii
LIST OF TABLES.....	x
LIST OF FIGURES	xi
LIST OF ABBREVIATIONS.....	xiii
CHAPTER	
1. INTRODUCTION	1
2. BASICS OF RADAR SIGNAL PROCESSING	5
2.1 Classical Radar Signal Processing Algorithms.....	6
2.1.1 Pulse Compression.....	6
2.1.2 Doppler Processing	8
2.1.2.1 MTI.....	9
2.1.2.2 Pulsed Doppler Processing	12
2.1.2.3 Moving Target Detector MTD.....	16
2.1.3 Threshold Detection.....	17
2.1.3.1 CA CFAR	18
2.1.3.1.1 CFAR Loss	20
2.1.3.1.2 Disadvantages of CA CFAR.....	21
2.1.3.1.3 Extensions to CA CFAR.....	23
2.1.3.2 OS CFAR.....	26
2.2 Non Gaussian Distributions and GLRT-LQ Detector	30
2.2.1 Non Gaussian Distributions.....	30
2.2.2 GLRT-LQ Detector	31
3. PROPOSED ALGORITHM.....	38

3.1 Doppler Processing Method Used in Analysis	39
3.1.1 Obtaining Interference Covariance Matrix.....	39
3.1.2 Comparison of GLRT-LQ Doppler Processor with MTI-DFT	42
3.2 Doppler Spreading Concept.....	44
3.3 Description of DPM.....	46
3.3.1 Details of the Algorithm	48
3.3.1.1 Obtaining Doppler Patterns	48
3.3.1.2 Flow of Algorithm	50
3.4 Comments on Proposed Algorithm	53
4.SIMULATIONS	54
4.1 Simulation Information.....	54
4.1.1 Radar Data Simulator	55
4.1.2 Processing Parameters	57
4.2 Simulation Results	58
4.2.1 Simulations without Target.....	59
4.2.2 Simulations with Single Target	59
4.2.2.1 Range Analysis	60
4.2.2.1.1 CA CFAR Range Analysis	60
4.2.2.1.2 SOCA CFAR Range Analysis	63
4.2.2.1.3 GOCA CFAR Range Analysis	65
4.2.2.1.4 OS CFAR Range Analysis.....	67
4.2.2.2 Doppler Analysis	69
4.2.3 Simulations with Two Targets.....	74
4.2.3.1 Scenario 1	75
4.2.3.2 Scenario 2	76
4.2.3.3 Scenario 3	78
5. CONCLUSIONS	80
REFERENCES	84

LIST OF TABLES

Table 2.1 Properties of Some Common Data Windows	16
Table 4.1 Simulation result of the scenario without target	59
Table 4.2 CA CFAR simulation result of the scenario with a single target.....	61
Table 4.3 Simulation result of the scenario with a single target	62
Table 4.4 SOCA CFAR simulation result of the scenario with a single target.....	64
Table 4.5 GOCA CFAR simulation result of the scenario with a single target.....	66
Table 4.6 OS CFAR simulation result of the scenario with a single target	68
Table 4.7 Properties of target in the Scenario 1	75
Table 4.8 Simulation results of Scenario 1	76
Table 4.9 Properties of target in the Scenario 2	76
Table 4.10 Simulation results of Scenario 2	78
Table 4.11 Properties of target in the Scenario 3	79
Table 4.12 Simulation results of Scenario 3	79

LIST OF FIGURES

Figure 2.1 Block Diagram of Generic Radar Signal Processing Algorithms	5
Figure 2.2 Autocorrelation Function of Length 13 Barker Code.....	8
Figure 2.3 MTI filter response and clutter spectra.....	10
Figure 2.4 An example of 8 pulse frequency response Doppler filter bank	12
Figure 2.5 Magnitude of the DTFT of an ideal moving target data sequence with FD = PRF/4 and 20 pulses, without window	14
Figure 2.6 Magnitude of the DTFT of an ideal moving target data sequence with FD = PRF/4 and 20 pulses, with Hamming window	15
Figure 2.7 MTD Signal Processor	17
Figure 2.8 Generic detection processor	18
Figure 2.9 Illustration of target masking	22
Figure 2.10 False alarm at clutter edge.....	23
Figure 2.11 Comparison of CA CFAR and SOCA CFAR with multiple targets and a clutter edge.....	24
Figure 2.12 Comparison of CA CFAR and GOCA CFAR with multiple targets and a clutter edge.....	26
Figure 2.13 Comparison of CA CFAR and OS CFAR with multiple targets and a clutter edge.....	29
Figure 2.14 P_D against SCR of GLRT-LQ and OGD detectors for fluctuating signal	36
Figure 2.15 P_D against SCR of GLRT-LQ, OGD and OD detectors for perfectly known signal.....	37
Figure 3.1 Baseband discrete-time equivalent system model.....	39
Figure 3.2 Response of one MTI+DFT filter and GLRT-LQ Doppler Filter	43
Figure 3.3 Maximum of responses for MTI+DFT and GLRT-LQ Doppler Filter. 43	43
Figure 3.4 An example of 8 pulse 1500 range bin Doppler processing output Doppler-Range matrix	45

Figure 3.5 Doppler spreading vectors.....	46
Figure 3.6 Data flow diagram of DPM.....	47
Figure 3.7 Doppler patterns	49
Figure 4.1 Shape of Babadağ Terrain	56
Figure 4.2 Autocorrelation function of pulse compression code that is used.....	57
Figure 4.3 SNR values	69
Figure 4.4 P_D values at close Doppler bin.....	71
Figure 4.5 P_D values at far Doppler bin before and after DPM	72
Figure 4.6 P_{FD} values before and after DPM.....	73
Figure 4.7 Base 10 logarithm of Improvement Factor.....	74

LIST OF ABBREVIATIONS

CA	Cell Averaging
CFAR	Constant False Alarm Rate
DPM	Doppler Pattern Matching
FIR	Finite Impulse Response
GLRT-LQ	Generalized Likelihood Ratio Test – Linear Quadratic
GOCA	Greatest of Cell Averaging
MTI	Moving Target Indicator
MTD	Moving Target Detector
OGD	Optimum Gaussian Detector
P_{FA}	Probability of False Alarm
P_{FD}	Probability of False Detection
P_D	Probability of Detection
PRI	Pulse Repetition Interval
SCR	Signal to Clutter Ratio
SNR	Signal to Noise Ratio
SOCA	Smallest of Cell Averaging

CHAPTER 1

INTRODUCTION

Fundamental purpose of radar is to detect targets. In order to achieve this, target echoes must be separated from interference echoes using radar signal processing algorithms. There are generic signal processing blocks common in radars.

First block that signal is passed through is Pulse Compression block. This block is simply a matched filter that maximizes Signal to Noise Ratio (SNR) for the pulse shape used in transmitted waveform.

After that, signal is passed through Doppler Processor block. At this block, there may be a single filter or a bank of filters, depending on the type of Doppler processor, in order to suppress clutter and noise echoes. Moving Target Indicator (MTI) is composed of a single filter which has a high pass response suppressing stationary clutter. Pulsed Doppler processor, on the other hand, is a bank of bandpass filters that passes certain parts of Doppler spectrum. It requires more pulses and processing power. However, it gives more idea about target, like target's radial velocity and number of targets. There is a method called Moving Target Detector (MTD) that uses both MTI and pulsed Doppler processing by making use of the digital signal processing technology.

Finally, data at the output of Doppler processor is compared with a predetermined threshold. If interference level is known and constant, this threshold may be set constant to keep probability of false alarm (P_{FA}) constant. However, usual case is that interference level is unknown and varying. Therefore, threshold should be

determined adaptively on runtime according to received signal. This way, P_{FA} can be kept constant. This is why; this type of detection is called CFAR detection.

If interference is independent, identically Gaussian distributed CA CFAR threshold achieves constant P_{FA} . CA CFAR uses the average of adjacent range cell signal level to estimate interference level and determine the threshold of a cell under test. In order to determine the threshold properly, interference level of adjacent cells should be the same with the interference level of the cell under test. Moreover, there should not be a target in these range cells. However, there are situations violating these conditions. Interference level can change abruptly on clutter edges; or two targets can be close to each other. At clutter edges, false alarms may increase at high level clutter region. In two target case, target with lower SNR can be masked with the threshold that is increased by target echo with higher SNR.

In order to compensate the performance degradation of CA CFAR at mentioned situations, extensions are brought to CA CFAR which are smallest of cell averaging (SOCA) CFAR and greatest of cell averaging (GOCA) CFAR. SOCA CFAR, calculates the average of adjacent range cells' signal level on two sides of the test cell separately and chooses the smaller one as the estimate of interference level. This way, target masking can be prevented but P_{FA} will increase. On the other hand, GOCA CFAR calculates the average of adjacent range cells' signal level on two sides of test cell separately like SOCA CFAR, but chooses the greater one as the estimate of interference level. This way, false alarms will reduce around clutter edges, but the rate of target masking will increase.

In [20], another CFAR method is proposed that functions well in mentioned exceptional situations. In this method, which is called ordered statistics (OS) CFAR, adjacent range cell data are rank ordered. Specific order of this sequence is selected as the estimate of interference. The trade off for the success of this algorithm is its algorithmic complexity. It requires much more processing power compared to CA CFAR.

The mentioned algorithms make use of the assumption that interference is Gaussian distributed. However, this is usually not the case, especially in high resolution radars. Therefore, non-Gaussian clutter models are proposed like K-distribution and Weibull distribution. Moreover, new processing algorithms are developed to function well in this type of interference. Generalized likelihood ratio test – linear quadratic (GLRT-LQ) detector, which assumes K-distributed interference, can be an example to such algorithms. GLRT-LQ includes both Doppler processing and threshold detection in its structure.

One problem that threshold detection algorithms suffer is ghosts. Ghost is a detection that results from target but at a point where there is no target. There are two main sources of ghosts. First one is the pulse compression which produces time sidelobes. If target echo is strong enough, sidelobes appear above noise floor. This may cause false detections at the transition regions of noise level and target side lobes. Doppler spreading is another source of ghosts. Because of the filter response of the Doppler filters, peaks may arise at the output of Doppler filters around target Doppler, which may cause ghosts.

In this thesis, a Doppler pattern matching (DPM) method is proposed to improve the performance of CA CFAR detection processor. This method makes use of Doppler spreading patterns that appears after Doppler processing. It is claimed that this method will reduce the false alarm and eliminate the ghosts resulting from Doppler spreading. On the other hand, it is not expected that ghosts resulting from pulse compression would be eliminated by this method.

This thesis is organized as follows. Chapter 2 is an overview of the mentioned radar signal processing algorithms. First, classical radar signal processing algorithms are described which are grouped into three as Pulse Compression, Doppler Processing and Threshold Detection. In the section about Doppler Processing, MTI, Pulsed Doppler Processing and MTD processor are explained. In the section on Threshold

Detection, CA CFAR, its extensions SOCA CFAR and GOCA CFAR and finally OS CFAR detection processors are handled. In the second part, two non-Gaussian interference distributions, which are Weibull distribution and K-distribution, are explained. Then, GLRT-LQ detector is investigated.

In Chapter 3, DPM is explained in details. There are comments on the situations where the algorithm works successfully.

In Chapter 4, there are simulations results that demonstrate the performance of DPM. Results are grouped into three; Simulations without Target, Simulations with Single Target and Simulations with Two Targets. In the section on “Simulations without Target”, false alarm reducing performance of DPM is investigated. In sections on “Simulations with Single Target” and “Simulations with Two Targets”, ghost and false alarm reducing performance of DPM is investigated in single target case and two target case respectively.

Chapter 5 includes some concluding remarks.

CHAPTER 2

BASICS OF RADAR SIGNAL PROCESSING

Radars radiate electromagnetic energy into space and receive echoes reflected from environment. Main objective of radar is detecting targets in echo signal and estimating some parameters of these targets like range and velocity. There are generic signal processing algorithms common in radars to achieve this purpose which can be seen in Figure 2.1.

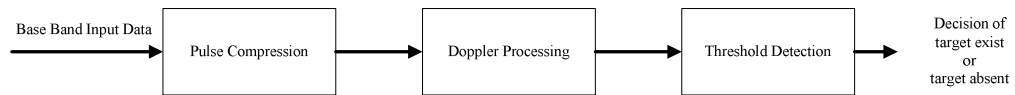


Figure 2.1 Block Diagram of Generic Radar Signal Processing Algorithms

In this thesis, two kinds of processing algorithms are investigated. First type of algorithms makes use of the assumption that clutter and noise are Gaussian distributed. These algorithms can be called classical radar signal processing algorithms. However, in some cases distribution deviates from Gaussian and classical methods fail. Therefore new methods are developed that will work successfully in environments with non Gaussian distributed clutter. In second part of this chapter, non-Gaussian distributions will be studied. Then, GLRT-LQ detector, which is designed to have a good performance in non-Gaussian distributed clutter, will be examined.

2.1 Classical Radar Signal Processing Algorithms

2.1.1 Pulse Compression

High range resolution is a desired property in radar. In order to achieve this, short pulses should be used which implies the use of large spectral bandwidth. It is advantageous to use short pulses in Signal to Clutter Ratio (SCR) sense since clutter power reduces in echo signal as pulse shortens. However, high peak power is necessary to achieve short-duration pulses. It is practically difficult to obtain high peak powers especially in high resolution cases. A long pulse can have same spectral bandwidth as a short pulse if the long pulse is modulated in frequency or phase [1]. This technique is called pulse compression.

Range resolution in radar is

$$\Delta R = \frac{cT}{2} \quad (2.1)$$

where T is the pulse duration and c is the speed of light ($3 \times 10^8 \text{ m/s}$). If pulse compression method is used range resolution becomes

$$\frac{c\tau}{2} \quad (2.2)$$

where τ is the chip length or in other words compressed pulse length. T/τ is the pulse compression ratio. Since signal bandwidth is approximately equal to $1/\tau$, then pulse compression ratio becomes time bandwidth product.

Pulse compression is carried out by filtering the echo of the transmitted signal that is composed of modulated pulses with duration T . Filter used at the receiver is a special filter that is called matched filter. Matched Filter is a linear filter that maximizes SNR at the output of filter for the pulse shape used. If we call pulse

shape function $p(n)$ and its length N , matched filter is time reversed pulse shape under additive white Gaussian noise assumption, i.e.

$$h(n) = p(N - n) \quad (2.3)$$

There are some other applications that use techniques like inverse filter, but those are not considered in this thesis.

There are two main figures of merit that characterizes the compressed signal [7]:

- Peak Sidelobe Level(PSL) = $10\log(\text{maximum sidelobe power/ peak power})$
- Integrated Sidelobe Level(ISL) = $10\log(\text{total power in the sidelobes/ peak power})$

Barker codes are common examples to binary phase modulated pulse shapes. Length 13 Barker Code is [7]:

$$[1,1,1,1,1,-1,-1,1,1,-1,1,-1,1]. \quad (2.4)$$

Its PSL is -22.3 dB, ISL is -11.5 dB and has an autocorrelation function as shown in Figure 2.2.

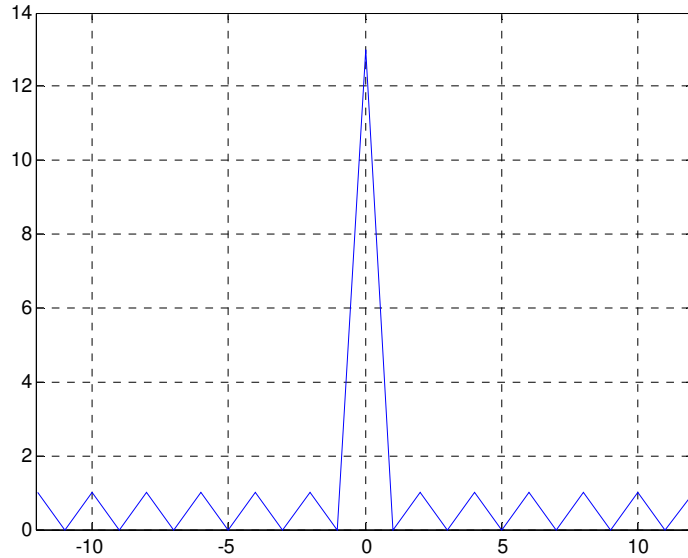


Figure 2.2 Autocorrelation Function of Length 13 Barker Code

2.1.2 Doppler Processing

The Doppler effect is a shift in the frequency of a wave radiated, reflected, or received by an object in motion [9]. It can be derived from rate of change of the phase. A received echo signal contains reflections from clutter, targets and noise. Each of these reflections has different Doppler characteristics. Clutter and noise signals have zero or little Doppler frequency compared to target signal.

Calling target range R and transmitted wavelength λ , total phase change in the two way propagation path is then

$$\phi = 2\pi \times \frac{2R}{\lambda} = 4\pi R / \lambda \quad (2.5)$$

Differentiating Eq.(2.5) with respect to time gives the rate of change of phase, which is the angular frequency:

$$\omega_d = \frac{d\phi}{dt} = \frac{4\pi}{\lambda} \frac{dR}{dt} = \frac{4\pi v_r}{\lambda} = 2\pi f_d \quad (2.6)$$

From the Eq.(2.6), Doppler frequency f_d can be extracted, which is [1]:

$$f_d = \frac{2v_r}{\lambda} = \frac{2f_t v_r}{c} \quad (2.7)$$

Target detection can be achieved by means of Doppler effect. MTI is an older and simpler method to achieve this, whereas Pulsed Doppler Processing is a more complicated method but it provides more information about target. Finally, MTD is a technique that combines both MTI and Pulsed Doppler Processing.

2.1.2.1 MTI

Aim of Doppler Processing is basically separating stationary signals from Doppler shifted signals. Since stationary signals are considered to be constant from pulse to pulse, this can be simply be achieved by subtracting echoes from pairs of pulses. As a result stationary signals would cancel out and target signal would not since it has phase changes. This process, in fact, is a linear high pass filter rejecting signals around zero frequency, whose transfer function, for a two pulse canceller is [1]:

$$H(f) = 2 \sin(\pi f T_p) \quad (2.8)$$

Double delay line canceller is another frequently used MTI filter which is formed by cascading 2 single delay line cancellers whose transfer function is [1]:

$$H(f) = 4 \sin^2(\pi f T_p) \quad (2.9)$$

Frequency response of these MTI filters can be seen in Figure 2.3. Both two pulse canceller and three pulse canceller filters out most of the clutter signal. The three pulse canceller improves the null breadth in the vicinity of zero Doppler, but it does not improve the consistency response to moving targets at different Doppler shifts away from zero Doppler [2]. That is to say, the only information that can be acquired from the data at output of the MTI is the existence of target. MTI fails in providing knowledge about number of detected targets or Doppler frequency of targets. In spite of this, MTI is a very simple algorithm to implement.

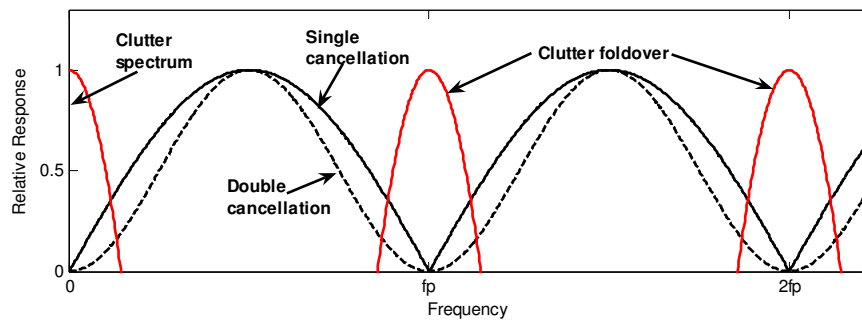


Figure 2.3 MTI filter response and clutter spectra [14]

There are two basic figures of merit for MTI [1]:

1. Clutter Attenuation
2. Improvement factor.

Clutter Attenuation is the ratio of the input clutter power to the output clutter power, which is defined as $CA = (C_i / C_o)$, is equal to

$$CA = \frac{\int_0^{\infty} W(f) df}{\int_0^{\infty} W(f) |H(f)|^2 df} \quad (2.10)$$

where $W(f)$ is PSD of the clutter and $H(f)$ is the frequency response of the MTI filter. When this formula is derived for two pulse canceller, assuming that the clutter is Gaussian distributed, it reduces to:

$$\frac{0.5}{1 - \exp(-2\pi^2 T_p^2 \sigma_c^2)} \quad (2.11)$$

where T_p is the pulse repetition interval and, σ_c is the standard deviation of the clutter spectral width. If the exponent term $2\pi^2 T_p^2 \sigma_c^2 \ll 1$, using $e^{-x} \approx 1 - x$ [14]:

$$CA \approx \frac{f_p^2}{4\pi^2 \sigma_c^2} \quad (2.12)$$

If a similar derivation is done for three pulse canceller, Clutter Attenuation becomes [14]:

$$CA \approx \frac{f_p^4}{48\pi^4 \sigma_c^4} \quad (2.13)$$

Clutter attenuation can be increased by using higher order delay line filters but at the expense of desired signal power [8].

2.1.2.2 Pulsed Doppler Processing

Pulse Doppler processing is a complex processing method compared to delay line cancellers. It is composed of bank of filters rather than a single filter. Each filter is a band pass filter that passes a certain frequency spectrum parts of the input signals.

To minimize the loss in SNR occurring when adjacent filters straddle a target's frequency, the center frequencies of the filters are spaced so the passbands overlap [6]. Frequency response of a filter bank composed of 8 filters can be an example to this property, which can be seen in Figure 2.4.

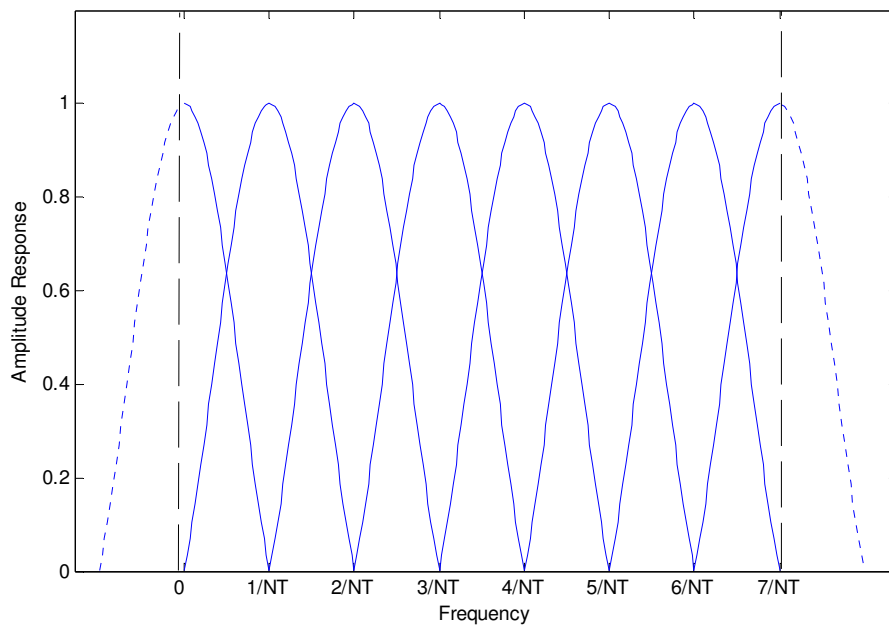


Figure 2.4 An example of 8 pulse frequency response Doppler filter bank

What is obtained at the output of filter bank is a range versus Doppler frequency matrix. Each point of matrix is compared with a threshold in order to detect targets. Complexity of pulsed Doppler processing brings some advantages. Multiple targets

can be resolved if they have different Doppler frequencies, because they will appear at the output of different filters. Moreover, the filter at which target is detected gives an idea about the radial velocity of target. Furthermore, because Doppler filters are narrowband compared to delay line cancellers, they are better at noise exclusion.

It is common to use Discrete Fourier Transform (DFT) as Pulsed Doppler Processor since they sample input signals in frequency domain. DFT is carried out by Fast Fourier Transform (FFT), which is a fast computing algorithm compared to original DFT calculation.

DFT is a processor that samples the signal in frequency domain using finite number of time samples. Moreover, no weighting is applied to these time samples, in other words, rectangular window is used. As a result of using finite number samples, spectral leakage occurs, where a signal having a single frequency shows up in more than one spectral bin [15]. In Figure 2.5 magnitude response of the DFT of a target with a nonzero Doppler frequency can be seen.

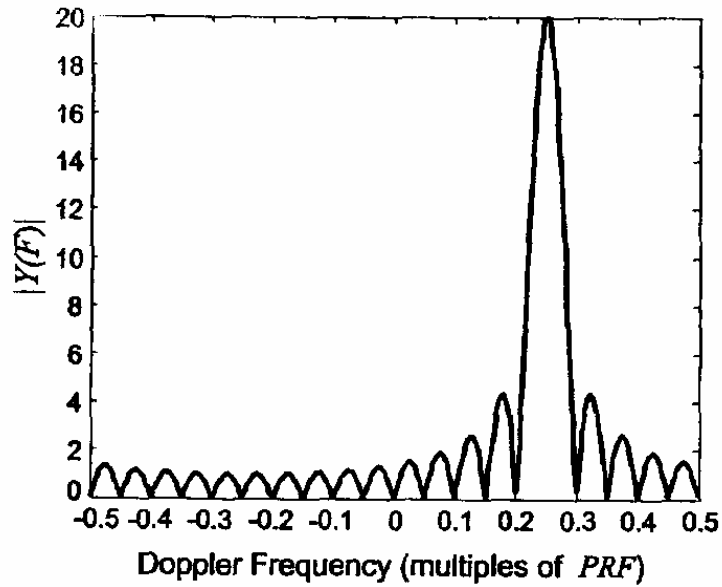


Figure 2.5 Magnitude of the DTFT of an ideal moving target data sequence with $FD = PRF/4$ and 20 pulses, without window [2]

Its mainlobe is narrow, which is a good property. However sidelobes are high, in other words spectral leakage is high. The rectangular window has the narrowest mainlobe for a given length, but it has the largest sidelobe of all commonly used windows [10]. This is because rectangular window simply turns the signal on and shut it off. More abruptly the time signal's amplitude changes, the higher spectral leakage [15]. In order to reduce sidelobes, windows other than rectangular, such as Hamming, Kaiser or Bartlett windows can be used, magnitude response of the DFT weighted with Hamming window can be observed in Figure 2.6.

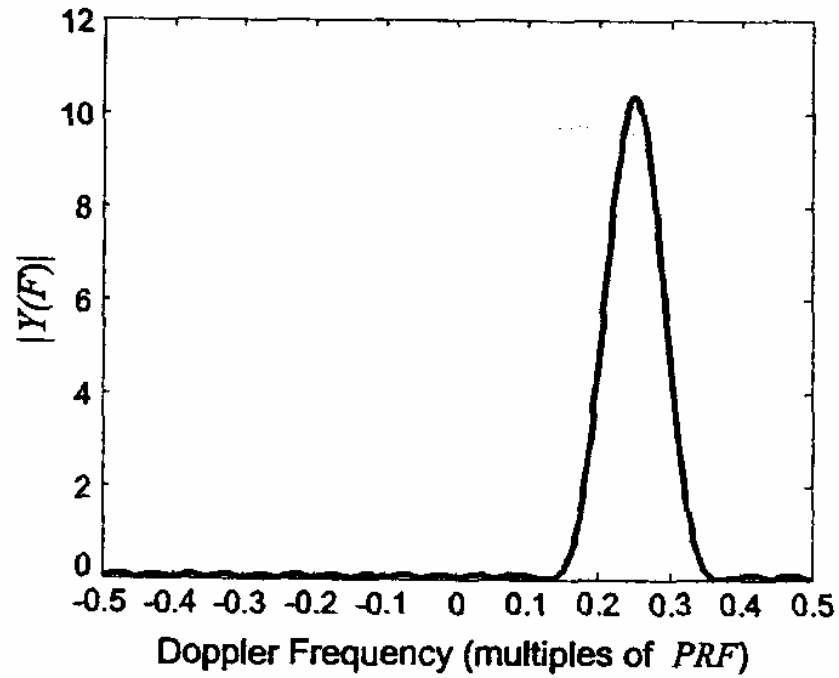


Figure 2.6 Magnitude of the DTFT of an ideal moving target data sequence with $FD = PRF/4$ and 20 pulses, with Hamming window [2]

As observed from the Figure 2.5 and Figure 2.6, mainlobe gets wider, peak magnitude reduces by 5.4dB but sidelobe level reduces by about 10dB. Consequently, there is a tradeoff between low sidelobe and mainlobe width.

Properties of some common windows can be observed in Table 2.1. The data in this table is taken from [22].

Table 2.1 Properties of Some Common Data Windows [22]

Window	Mainlobe width	Peak gain (dB)	Peak side lobe, dB	SNR loss, dB
Rectangular	1.0	0.0	-13	0
Hann	1.62	-6.0	-32	-1.76
Hamming	1.46	-5.4	-43	-1.35
Kaiser, $\alpha = 2.0$	1.61	-6.2	-46	-1.76
Kaiser, $\alpha = 2.5$	1.76	-8.1	-57	-2.17
Dolph-Chebyshev (50-dB equiripple)	1.49	-5.5	-50	-1.43
Dolph-Chebyshev (70-dB equiripple)	1.74	-6.9	-70	-2.10

2.1.2.3 Moving Target Detector MTD

With the usage of digital signal processor in radars, it became possible to implement complex processing algorithms compared to those that can be accomplished with analog processors. Moving Target Detector is an algorithm that takes the advantage of digital signal processors and combines both MTI and Pulsed Doppler Processing techniques. Original MTD was designed in MIT Lincoln Library for ASR-8 Air Surveillance Radar [1]. Its block diagram can be seen in Figure 2.7.

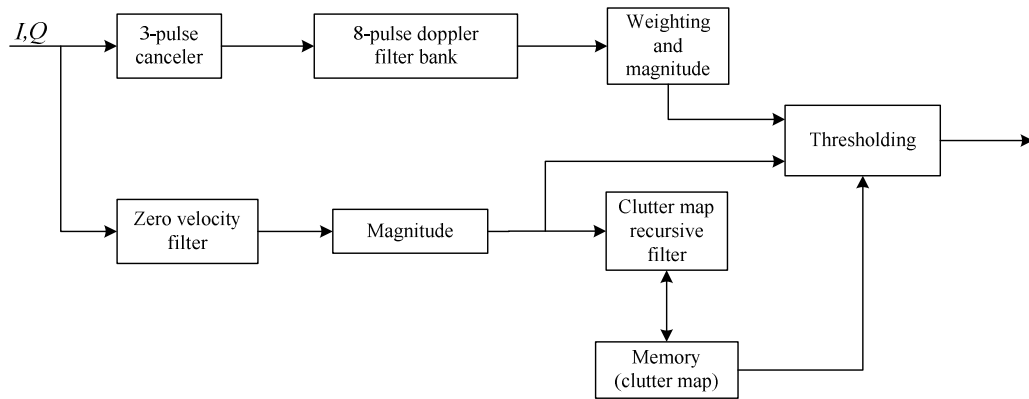


Figure 2.7 MTD Signal Processor [1]

Three pulse canceller was used to remove stationary clutter contribution to echo signal, so that signal at the output of MTI block would be mainly composed of moving target and moving clutter echoes and noise at the output of MTI block. After the MTI block, multiple moving targets and moving clutter could be resolved by 8 pulse FFT block if they appeared at different Dopplers. In order to reduce the sidelobes of FFT, weighting is applied to the output of Doppler-filter block. Finally, threshold detection is performed to decide existence of target.

After the original MTD, more complicated MTD processors were designed as the technology improved. FFT were replaced with Finite Impulse Response (FIR) banks. FIR filter banks had lower sidelobes and provided flexibility in design since each filter in the bank could have desired frequency response. Moreover, bit depth of the filters were increased which is another factor that reduces sidelobes. Furthermore, different numbers of pulses were used for different pulse repetition intervals to cover similar Doppler spaces at different Pulse Repetition Intervals (PRI).

2.1.3 Threshold Detection

In a common detection processor like that shown in Figure 2.8, data at the output of the Doppler processor is first passed through a square law, linear or log detector.

Then this data is compared to a threshold to decide existence of a target. This threshold may be constant or may be adaptive.

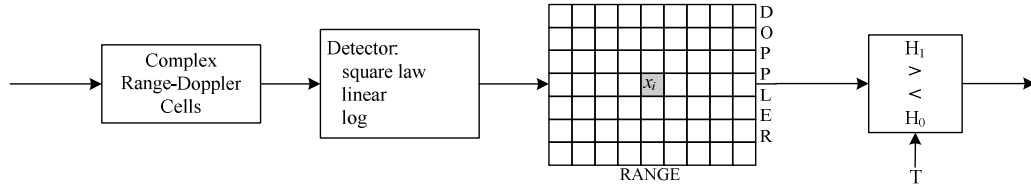


Figure 2.8 Generic detection processor [2]

In constant threshold case, it is assumed that interference level is known and threshold is fixed according to that level and required P_{FA} . However, in radars interference level is usually unknown and variable. Therefore, P_{FA} would be unpredictable which is an undesirable case. In order to achieve stable performance, P_{FA} is preferred to be constant. To achieve this, the actual interference power must be estimated from data in real time, so that the detector threshold can be adjusted to maintain desired probability of false alarm [2]. This kind of detector is called (constant false alarm rate) CFAR detector. In this thesis, two types of CFAR detector, namely Cell Averaging CFAR (CA CFAR) and Order Statistics CFAR (OS CFAR) algorithms are studied.

2.1.3.1 CA CFAR

After Doppler processing block, a range versus Doppler data matrix is obtained. For each data in the matrix, a threshold should be determined according to the estimated interference power. CA-CFAR uses adjacent range data to achieve this with the following assumptions [2]:

- The neighboring cells contain interference with the same statistics as the cell under test, so that they are representative of the interference that is competing with

the potential target.

- The neighboring cells do not contain any targets; they contain only interference.
- Interference is independent and identically distributed. This distribution is Gaussian distribution.

With further assumption that asquare law detector being used, using maximum likelihood estimation interference power $\hat{\beta}^2$ would be:

$$\hat{\beta}^2 = \frac{1}{N} \sum_{i=1}^N x_i \quad (2.14)$$

where x_i is the power of signal since square law detector is used.

The required threshold is then estimated as a multiple of the estimated interference power, where α is the scale factor [2]:

$$\hat{T} = \alpha \hat{\beta}^2 \quad (2.15)$$

Combining the equations (2.14) and (2.15) estimation of the required threshold becomes the average of N neighboring range cells, scaled with α :

$$\hat{\beta}^2 = \frac{\alpha}{N} \sum_{i=1}^N x_i \quad (2.16)$$

The purpose of using adaptive threshold is to have a predictable performance. Since interference is a random variable, an analytical formula for the estimate of $P_{FA}(\bar{P}_{FA})$ can be obtained. Scale factor α and number of averaged cells N are the parameters that are effecting \bar{P}_{FA} . For the square law case, it is[2]:

$$\bar{P}_{FA} = \left(1 + \frac{\alpha}{N}\right)^{-N} \quad (2.17)$$

A formula for the estimate of probability of detection (P_D) can be obtained that depends also on SNR where SNR is denoted by χ [2]:

$$\bar{P}_D = \left(1 + \frac{\alpha}{N(1+\chi)}\right)^{-N} \quad (2.18)$$

Sometimes target echo may spread to a few range cells. In this case it would be inappropriate to use these cells to estimate the interference. Therefore a few range cells that are closest to the test cell is discarded. These cells are called guard cells.

2.1.3.1.1 CFAR Loss

The greater the number of reference cells in the CA CFAR the better is the estimate of the background clutter [1]. However, there is a practical limit to this number; signal processor can process a limited amount of data. So, there is loss resulting from using finite number data. This loss is called CFAR loss.

When N cells are used to estimate the interference, required SNR with predetermined probabilities is [2]

$$\chi_N = \frac{\left(\bar{P}_D / \bar{P}_{FA}\right)^{1/N} - 1}{1 - \bar{P}_D^{1/N}} \quad (2.19)$$

When infinitely many samples are used, it is [2]

$$\chi_{\infty} = \frac{\ln(\overline{P}_{FA} / \overline{P}_D)}{\ln(\overline{P}_D)} \quad (2.20)$$

CFAR loss is formulated as the ratio of SNR required with finite number of samples to the SNR required with infinitely many samples, which is [2]:

$$\text{CFAR loss} = \frac{\chi_N}{\chi_{\infty}} \quad (2.21)$$

2.1.3.1.2 Disadvantages of CA CFAR

In Section 2.4.1, it was stated that CA CFAR has two main assumptions. First one was that there is no target in the cells that are used to estimate interference power. Second one was that the interference is independent and identically distributed. CA CFAR fails in some cases because of these assumptions.

In Figure 2.9, failure of CA CFAR due to the first assumption can be observed. Interference level is 20dB, the target in range bin 50 has an SNR of 15 dB, and the threshold is computed using 20 range cells and a desired \overline{P}_{FA} of 10^{-3} . However, a second target with an SNR of 20dB in range bin 58 elevates the estimated interference power when the first target is in the test cell. This increase in threshold is sufficient to prevent detection of the first target in this case. On the other hand, the 15dB target does not affect the threshold enough to prevent the detection of the second, stronger target [12]. Shortly to say, first target is masked by the second target.

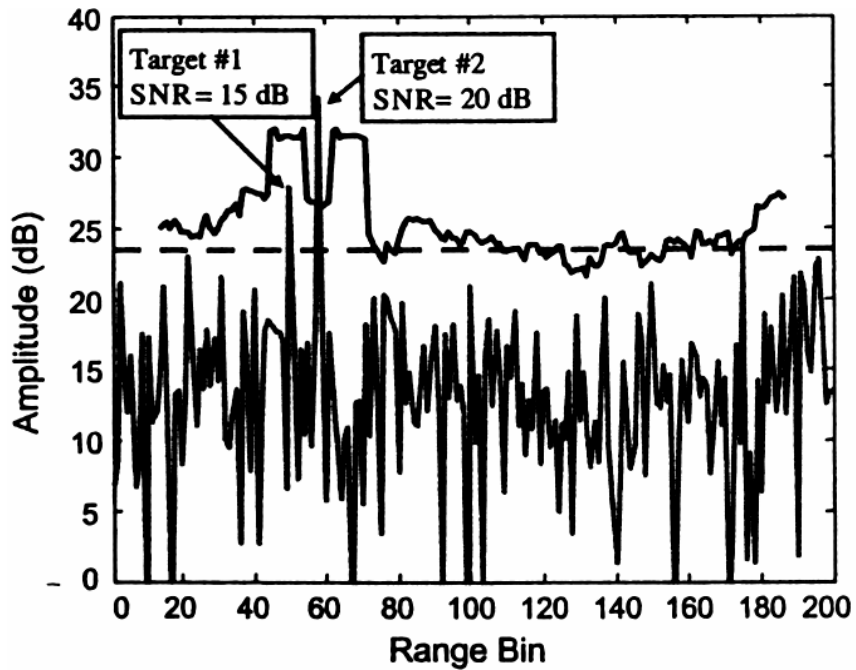


Figure 2.9 Illustration of target masking [2]

In Figure 2.10, failure of CA CFAR because of the second assumption can be observed. In the first 100 bins, interference level is about 20 dB. Around range bin 100, there is a sharp increase of about 10dB in interference level. Therefore, threshold determinations around range cell 110 are not appropriate and detection at range cell 113 is affected. Because of low level data at the beginning of CFAR window, interference level is estimated lower compared to actual case. So, a false alarm occurred at range cell 113.

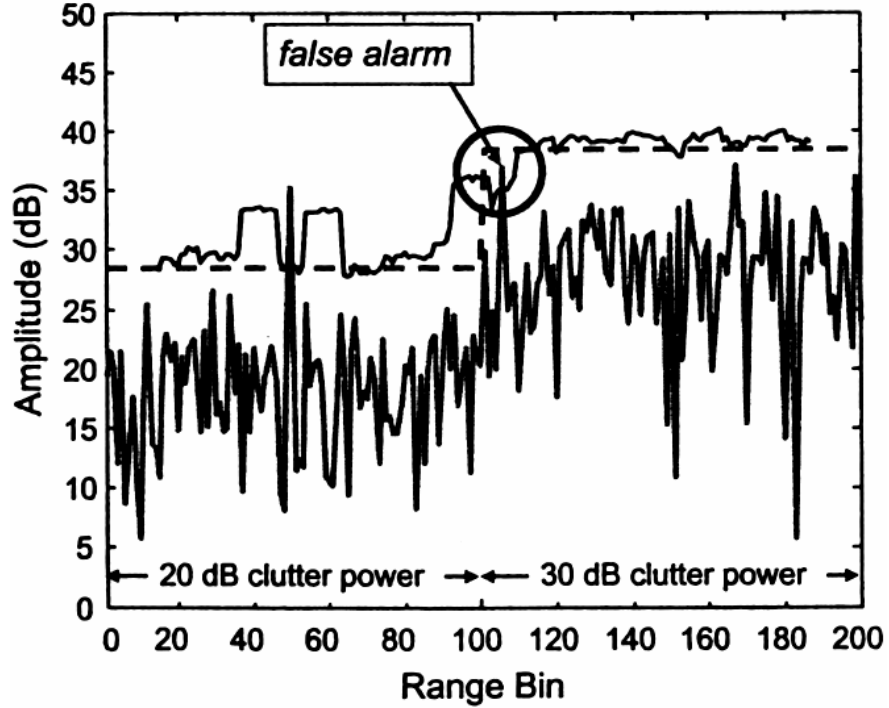


Figure 2.10 False alarm at clutter edge [2]

2.1.3.1.3 Extensions to CA CFAR

Some extensions are brought to CA CFAR technique, in order to compensate performance reduction of this technique. In this thesis, GOCA(Greatest of Cell Averaging) CFAR and SOCA(Smallest of Cell Averaging) CFAR extensions are studied.

In CA CFAR technique, range cells on either side of test cell are averaged. In GOCA CFAR and SOCA CFAR techniques, the average of data on either side is calculated separately. SOCA CFAR selects the smaller of these two averages to determine the threshold whereas GOCA CFAR selects the greater of these two averages, then multiplies it with a scale factor, to determine the threshold [12]:

$$\hat{T}_{GO} = \alpha_{GO} \max(\hat{\beta}_1^2, \hat{\beta}_2^2) \quad (2.22)$$

$$\hat{T}_{SO} = \alpha_{SO} \min(\hat{\beta}_1^2, \hat{\beta}_2^2) \quad (2.23)$$

α_{GO} is the scale factor of GOCA CFAR and α_{SO} is the scale factor of SOCA CFAR. $\hat{\beta}_1^2$ and $\hat{\beta}_2^2$ are lagging and leading averages respectively.

SOCA CFAR is a preferred technique to prevent misses resulting from target masking. This can be observed in Figure 2.11. Second target is below CA CFAR threshold, but it stays above SOCA CFAR threshold. The price paid for this detection is the increase in the P_{FA} , especially around clutter crossing. Therefore, this method is appropriate to use in homogeneous environments.

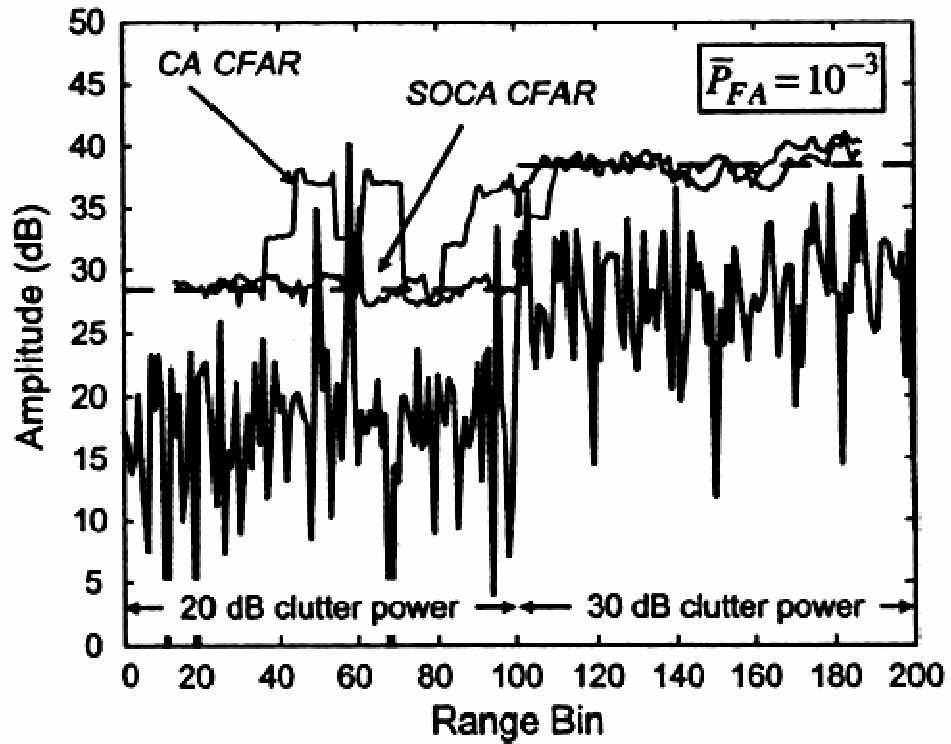


Figure 2.11 Comparison of CA CFAR and SOCA CFAR with multiple targets and a clutter edge [2]

An expression for the estimate of P_{FA} as a function of N and α for SOCA CFAR has been obtained as [16]

$$\bar{P}_{FA/2} = \left(2 + \frac{\alpha}{(N/2)} \right)^{-N/2} \left\{ \sum_{k=0}^{\frac{N}{2}-1} \binom{\frac{N}{2}-1+k}{k} \left(2 + \frac{\alpha}{(N/2)} \right)^{-k} \right\} \quad (2.24)$$

GOCA CFAR, on the other hand, is method that compensates performance degradation resulting from the assumption that interference is independent and identically distributed. As stated above, this will cause false alarms around clutter edges in CA CFAR technique. On the other hand, GOCA CFAR would choose the estimation with the higher value, so that false alarms would not occur. This behavior can be observed in Figure 2.12. The drawback of this technique is that it has a target masking behavior worse than CA CFAR. It is expected, since GOCA CFAR's threshold is larger than CA CFAR's threshold.

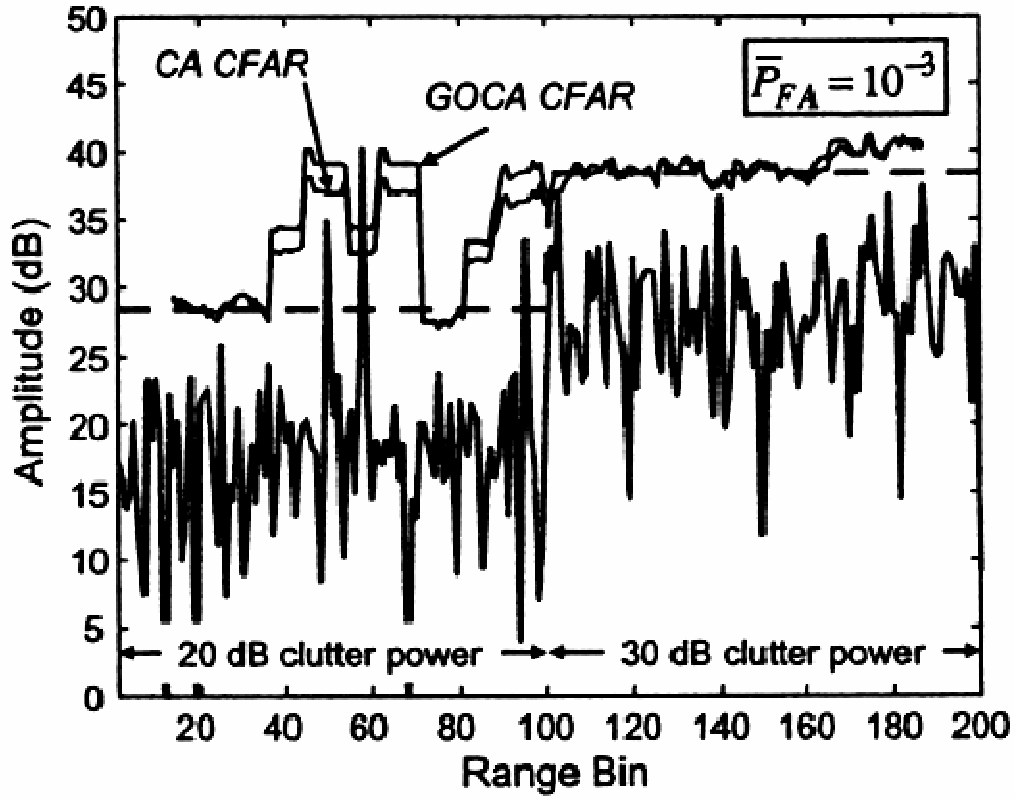


Figure 2.12 Comparison of CA CFAR and GOCA CFAR with multiple targets and a clutter edge [2]

An equation for the estimate of P_{FA} can be obtained for GOCA CFAR also that has dependency on N and α [16]:

$$\bar{P}_{FA/2} = \left(1 + \frac{\alpha_{GO}}{(N/2)}\right)^{-N/2} - \left(2 + \frac{\alpha_{GO}}{(N/2)}\right)^{-N/2} \left\{ \sum_{k=0}^{\frac{N}{2}-1} \binom{N}{2k} \left(\frac{N}{2} - 1 + k\right) \left(2 + \frac{\alpha_{GO}}{(N/2)}\right)^{-k} \right\} \quad (2.25)$$

2.1.3.2 OS CFAR

CA CFAR detectors use average of adjacent cells to estimate interference power. There is another detector called OS CFAR that uses another way to estimate

interference power. OS CFAR selects a window of length N , which are adjacent to the range cell of interest, as in the case of CA CFAR. The data in this window are rank ordered and a sequence is formed like $\{x_1, x_2, \dots, x_N\}$. k^{th} order of this sequence, x_k is used as the estimate of interference and the threshold is set to a multiple of this value:

$$\hat{T} = \alpha_{OS} x_k \quad (2.26)$$

where α_{OS} is the scale factor [2].

Motivation of this algorithm comes from the rank-order operators that are used for image filtering. The sliding window of the radar CFAR system corresponds to the local operator as used in image processing. The calculation of a threshold value individually for every test cell is identical to generation of a threshold image with the dimensions and the resolution of the input image. In image processing, the local operator is called a rank-order operator if it outputs a preselected value from the ordered statistic [20].

In order to be called CFAR, P_{FA} of a detector should be independent of interference power. P_{FA} for OS CFAR detector is given by

$$P_{FA} = P[Y_0 \geq \alpha_{OS} x_k] \quad (2.27)$$

where Y_0 is a noise sample with exponential distribution [20].

Probability density function of the k^{th} value of the ordered statistic for exponentially distributed random variable with mean value μ is [20]

$$p_k(x) = k/\mu \binom{N}{k} (e^{-x/\mu})^{N-k+1} (1 - e^{-x/\mu})^{k-1} \quad (2.28)$$

Then P_{FA} can be obtained as

$$\begin{aligned}
P_{FA} &= \int_0^{\infty} P[Y_0 \geq \alpha_{OS} x] p_k(x) dx = \int_0^{\infty} e^{-\alpha_{OS} x / \mu} k / \mu \binom{N}{k} (e^{-x / \mu})^{N+1-k} (1 - e^{-x / \mu})^{k-1} dx \\
&= k \binom{N}{k} \int_0^{\infty} e^{-(\alpha_{OS} + N + 1 - k)y} (1 - e^{-y})^{k-1} dy \\
&= k \binom{N}{k} \frac{(k-1)! (\alpha_{OS} + N - k)!}{(\alpha_{OS} + N)!} \tag{2.29}
\end{aligned}$$

P_{FA} is independent of clutter parameters, therefore OS method satisfies CFAR property.

The choice of N and k determines the performance of OS-CFAR. A value of k greater than N/2 should be used in order to avoid false alarms at clutter edges. Typically, k is on the order of 0.75N [21]. In Figure 2.13, the performance of CA CFAR is compared with OS CFAR. N = 20 and k = 15th order statistics is used. The use of the ordered statistic instead of a mean estimate makes the detector almost completely insensitive to masking by closely spaced targets so long as the number of cells contaminated by interfering targets does not exceed N-k. In this example, both closely spaced targets are detected [2].

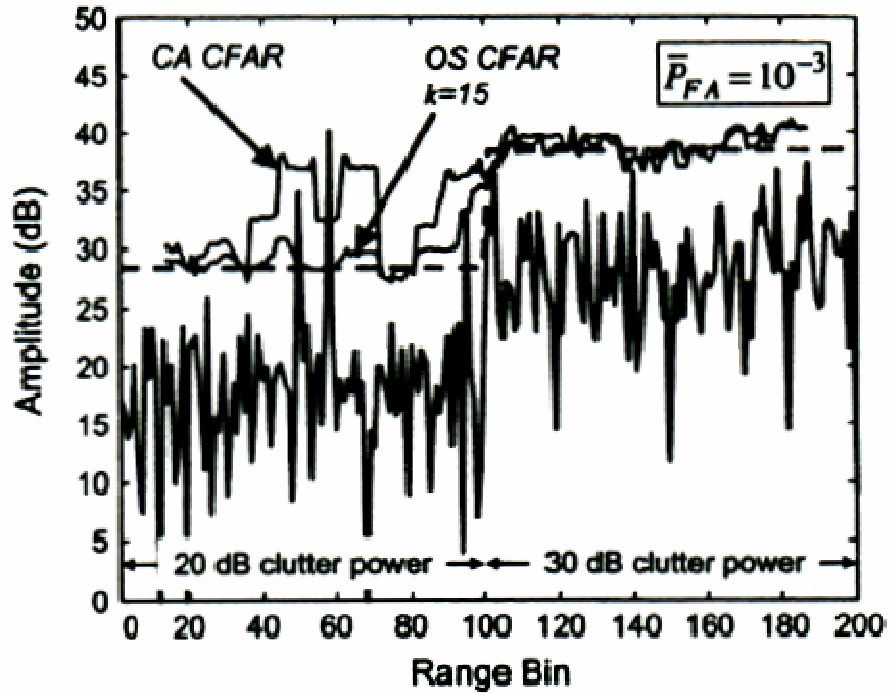


Figure 2.13 Comparison of CA CFAR and OS CFAR with multiple targets and a clutter edge [2]

In practical CA CFAR application, guard cells are used for separating the cell under test from the reference area in order to prevent target returns from falsifying the clutter level estimation. In OS CFAR processing these guard cells become unnecessary since small number of target amplitudes occurring within the reference area have almost no influence on the clutter level estimation by quantiles [20].

Despite the advantages, OS CFAR is a computationally heavy algorithm compared to CA CFAR. OS CFAR's computational complexity is $O_{OS}(n) = n \log(n)$ at the best case, whereas CA CFAR's computational complexity is $O_{CA}(n) = n$. Fortunately, with the improvement of digital technology, OS CFAR can practically be used.

2.2 Non Gaussian Distributions and GLRT-LQ Detector

Clutter is used to be modeled as Gaussian distributed random variable. However, clutter deviates from Gaussian especially in high resolution radars. Weibull distribution and K-distribution are two main distributions that clutter is assumed to have. These distributions are explained in Section 2.2.1.

GLRT-LQ detector is a detector that is designed to have a good performance both in Gaussian and non Gaussian distributed clutter. It comprises both Doppler processing and threshold detection in its structure. This detector is investigated in Section 2.2.2.

2.2.1 Non Gaussian Distributions

In this section non-Gaussian distributions K distribution and Weibull distributions will be explained.

The cumulative distribution function of the K-distribution is given by

$$P(x) = 1 - \frac{2}{\Gamma(\nu)} \left(\frac{d\sqrt{x}}{2} \right)^\nu K_\nu(d\sqrt{x}) \quad (2.30)$$

where Γ is the Gamma function and K_ν is the modified Bessel function of second kind of order ν . The parameter ν is the shape parameter of K-distribution and $1/d$ is a scale parameter [26].

The Weibull probability density function for the normalized amplitude $v_n = v/v_m$ is

$$p(v_n) = \alpha (\ln 2) v_n^{\alpha-1} \exp[-(\ln 2) v_n^\alpha] \quad v_n \geq 0 \quad (2.31)$$

where α is a parameter that relates to skewness of the distribution, and v_m is the median value of the distribution. When α is equal to 2, Weibull takes the form of Rayleigh distribution and when α is equal to 1 it is equal to exponential probability distribution function [1].

In [26] it is stated that, Weibull statistics usually provide better fits to the clutter amplitude distributions than K-distribution. Moreover, it is analytically simpler and more tractable than K- distribution.

2.2.2 GLRT-LQ Detector

GLRT-LQ detector assumes the disturbance to be a mixture of K-distributed clutter and Gaussian Clutter in [19]

$$\mathbf{d} = \mathbf{c} + \mathbf{c}_G + \mathbf{n} \quad (2.32)$$

Vectors \mathbf{d} , \mathbf{c} , \mathbf{c}_G and \mathbf{n} are m -dimensional vectors where m is the number of transmitted pulse. \mathbf{n} represents the Gaussian distributed thermal noise; \mathbf{c}_G represents the Gaussian distributed clutter; \mathbf{c} represents the non-Gaussian distributed clutter and finally \mathbf{d} represents the whole disturbance. If it is assumed that noise power is much lower than the clutter power than disturbance vector reduces to [17]:

$$\mathbf{d} = \mathbf{c} + \mathbf{c}_G \quad (2.33)$$

Non-Gaussian part of the clutter can be modeled as K-distributed random variable

$$\mathbf{c} = \sqrt{\tau} \mathbf{x} \quad (2.34)$$

where \mathbf{x} is an m -dimensional complex Gaussian circular random vector, usually named speckle, that represents the properties of the coherent radar sensor. The in phase (x_{Ii}) and quadrature (x_{Qi}) components are zero mean real random variables with unit variance and covariance matrix \mathbf{M}_x [17]:

$$E\{\mathbf{x}\mathbf{x}^H\} = 2E\{\mathbf{x}_I\mathbf{x}_I^T\} = 2E\{\mathbf{x}_Q\mathbf{x}_Q^T\} = 2\mathbf{M}_x \quad (2.35)$$

The variable τ , usually referred as texture, represents the local power of the clutter. It is assumed to be Gamma distributed, with mean value μ and order parameter ν since clutter is modeled as K-distributed [18]:

$$p_\tau(\tau) = \frac{1}{\Gamma(\nu)} \left(\frac{\nu}{\mu}\right)^\nu \tau^{\nu-1} e^{-\frac{\nu}{\mu}\tau}, \quad \tau \geq 0 \quad (2.36)$$

The order parameter ν demonstrates the spikiness property of the clutter. For small ν values like 0.2, the clutter is very spiky. As ν tends to infinity, K- distribution approaches to Gaussian. At value of 4.5, distribution is almost Gaussian [17].

The clutter term \mathbf{c}_G is characterized by a complex Gaussian circular PDF whose components are zero mean with variance $2\sigma_G^2$ and normalized covariance matrix \mathbf{M}_G . Given a specific τ , conditional covariance matrix of disturbance vector \mathbf{d} is given by [17]:

$$M_{d|\tau} \triangleq \frac{1}{2} E\{d d^H | \tau\} = E\{d_I d_I^T | \tau\} = E\{d_Q d_Q^T | \tau\} = \tau M_x + \sigma_G^2 M_G \quad (2.37)$$

It may be assumed that \mathbf{M}_G is equal to \mathbf{M}_x , $\mathbf{M} = \mathbf{M}_x = \mathbf{M}_G$. This assumption reduces computational effort; meanwhile it has a physical justification. While the texture variable represents the characteristics of the observed scene, the speckle takes into account coherent sensor effects. In these terms the correlation structure of

the speckle is independent of texture distribution. The two matrices are generated by the same phenomenon, the antenna rotation, so they are almost identical [19].

With the assumption stated above, the unconditional PDF of \mathbf{d} is obtained by averaging $p_{d|\tau}(d|\tau)$ with respect to texture distribution $p_\tau(\tau)$ [17]:

$$p_d(d) = \int_0^\infty \frac{1}{(2\pi)^m (\tau + \sigma_G^2) |\mathbf{M}|} \times \exp\left[-\frac{d^H \mathbf{M}^{-1} d}{2(\tau + \sigma_G^2)}\right] p_\tau(\tau) d\tau \quad (2.38)$$

Under Neyman-Pearson criterion, optimum detection procedure is carried out by comparing the likelihood ratio of two hypotheses H_0 and H_1 with a predetermined threshold λ according to desired P_{FA} . In hypotheses H_0 , data is composed of only disturbance and the PDF is given by $p_Z(z|H_0) = p_d(z)$. In hypotheses H_1 , data is composed of disturbance and signal $\mathbf{s} = \alpha \mathbf{p}$, where α is a complex parameter that can be known or unknown and \mathbf{p} is a perfectly known vector with components $p_i = e^{j2\pi f_D T}$, T being the PRI and f_D is the target Doppler frequency. Resulting PDF is $p_Z(\mathbf{z}|H_1) = p_d(\mathbf{z} - \mathbf{s})$. If signal assumed to be perfectly known, then the resulting optimum strategy is [17]:

$$\int_0^\infty (\tau + \sigma_G^2)^{-m} \left[\exp\left(-\frac{q_1(\mathbf{z})}{2(\tau + \sigma_G^2)}\right) - \lambda \exp\left(-\frac{q_0(\mathbf{z})}{2(\tau + \sigma_G^2)}\right) \right] p_\tau(\tau) d\tau \underset{H_0}{\overset{H_1}{>}} 0 \quad (2.39)$$

where

$$q_0(\mathbf{z}) \triangleq \mathbf{z}^H \mathbf{M}^{-1} \mathbf{z} \quad (2.40 \text{ a})$$

$$q_1(\mathbf{z}) \triangleq (\mathbf{z} - \mathbf{s})^H \mathbf{M}^{-1} (\mathbf{z} - \mathbf{s}) = q_0(\mathbf{z}) - 2 \operatorname{Re}\{\mathbf{s}^H \mathbf{M}^{-1} \mathbf{z}\} + \mathbf{s}^H \mathbf{M}^{-1} \mathbf{s} \quad (2.40 \text{ b})$$

If the disturbance is completely Gaussian then the optimum detection strategy would be whitening matched filter compared to a fixed threshold which is called Optimum Gaussian Detector (OGD) [17].

In a more realistic case, signal can not be perfectly known, then it would be proper to model α as a random variable. If α is assumed to be Gaussian random variable with zero mean and variance $2\sigma_A^2$, then the optimum detection (OD) structure would be the same as in Eq (2.39) but $q_1(\mathbf{z})$ should be replaced with $q_2(\mathbf{z})$, which is [17]:

$$q_2(\mathbf{z}) \triangleq \frac{\mathbf{z}^H \mathbf{M}_{d|\tau}^{-1} \mathbf{z} (\mathbf{p}^H \mathbf{M}_{d|\tau}^{-1} \mathbf{p} + 4/\sigma_A^2) - |\mathbf{z}^H \mathbf{M}_{d|\tau}^{-1} \mathbf{z}|^2}{\mathbf{p}^H \mathbf{M}_{d|\tau}^{-1} \mathbf{p} + 4/\sigma_A^2} \quad (2.41)$$

In both cases, where signal is perfectly known and it is assumed to be fluctuating, knowledge of the clutter parameters, μ , ν and σ_G^2 is required.

In this situation a new sub-optimum approach is developed in [17]; maximum likelihood (ML) estimate of the texture component of K-distributed clutter will be used in the likelihood ratio test. For perfectly known signal, the detector structure would be:

$$(1 - \eta)q_0(\mathbf{z}) + 2\eta a(\mathbf{z}) - \eta c \quad (2.42)$$

where $a(\mathbf{z}) \triangleq \text{Re}\{\mathbf{s}^H \mathbf{M}^{-1} \mathbf{z}\}$, whitening matched filter, and $c \triangleq \text{Re}\{\mathbf{s}^H \mathbf{M}^{-1} \mathbf{s}\}$. The equation involves $q_0(\mathbf{z})$, which is quadratic statistics of input vector \mathbf{z} , so this GLRT detector structure is a linear quadratic system. Therefore it is called GLRT-LQ detector. It is much simpler than the optimum detector structure and does not depend on clutter parameters, μ , σ_G^2 and ν [17].

In a realistic scenario, signal amplitude $\alpha = Ae^{j\theta}$ would fluctuate, where A can be modeled as Rayleigh distributed and phase θ is modeled as uniformly distributed in $[0, 2\pi]$. With some mathematical manipulations, using ML estimates of α and τ , suboptimum receiver structure will reduce to [17]:

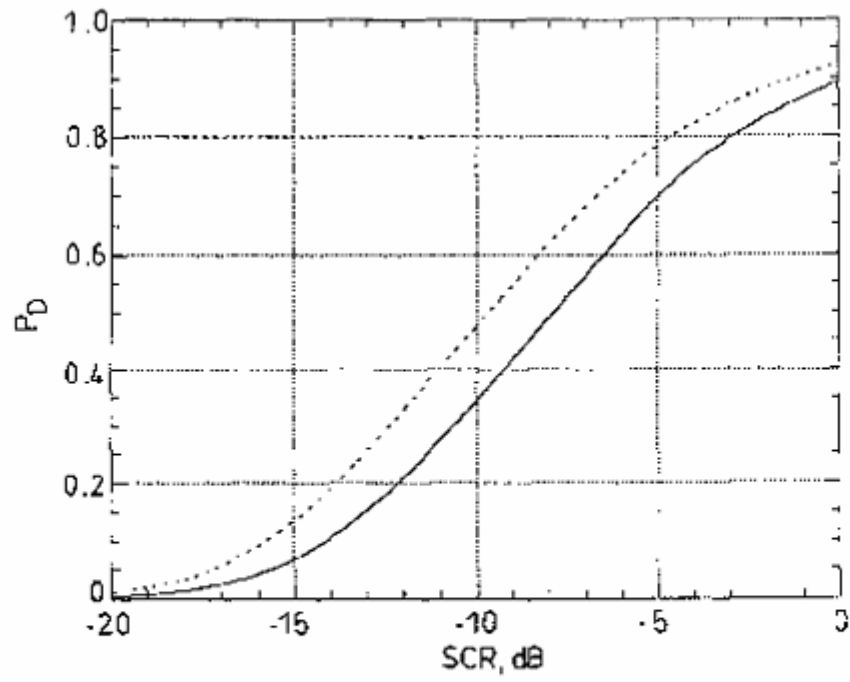
$$\frac{|\mathbf{p}^H \mathbf{M}^{-1} \mathbf{z}|^2}{(\mathbf{z}^H \mathbf{M}^{-1} \mathbf{z})(\mathbf{p}^H \mathbf{M}^{-1} \mathbf{p})} \underset{H_0}{\overset{H_1}{>}} \eta \quad (2.43)$$

This expression can be converted to another form

$$|\mathbf{p}^H \mathbf{M}^{-1} \mathbf{z}|^2 \underset{H_0}{\overset{H_1}{>}} (\mathbf{z}^H \mathbf{M}^{-1} \mathbf{z})(\mathbf{p}^H \mathbf{M}^{-1} \mathbf{p})\eta \quad (2.44)$$

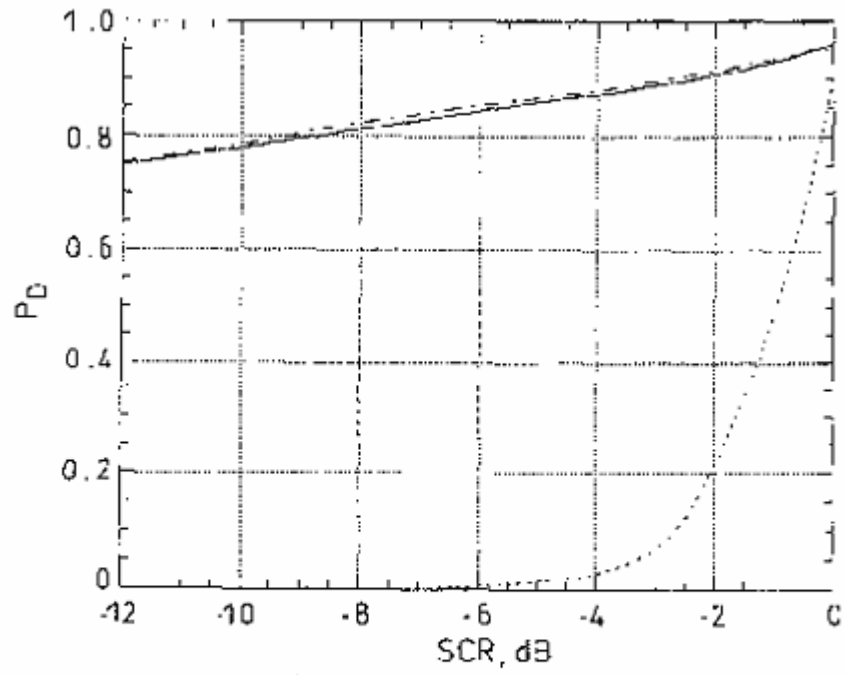
The term on the left hand side can be considered as a classical detector. \mathbf{M}^{-1} transformation applies MTI clutter suppression to signal. \mathbf{p}^H multiplication is the classical DFT Doppler processor [6]. Finally, magnitude square of the output signal is calculated which is similar to a square law detector. The term on the left hand side, is data dependent adaptive threshold. Adaptive property of the detector comes from the $(\mathbf{z}^H \mathbf{M}^{-1} \mathbf{z})$ term. This detection technique performs as the classical cell averaging CFAR detector operating in the Gaussian environment. The only difference is that GLRT-LQ detector estimates the clutter power by means of time samples from the range cell under test, while the CA CFAR detector usually utilizes spatial samples from adjacent range cells [17].

The performance of GLRT-LQ detector is almost equal to that of optimum receiver, particularly when the K-distributed clutter component predominates over the Gaussian component [17]. This can be observed in Figure 2.14 and Figure 2.15.



$P_{FA} = 10^{-3}$, $\mu = 0$, $\sigma_G^2 = 1000$, $\rho = 0.9$, $m = 16$, $f_D T = 0.5$
 OGD detector
 ——— GLRT-LQ detector

Figure 2.14 P_D against SCR of GLRT-LQ and OGD detectors for fluctuating signal [17]



$P_{FA} = 10^{-5}$, $\mu = 1000$, $\sigma_C^2 = 0$, $\nu = 0.1$, $\rho = 0.9$, $m = 16$, $f_0 T = 0.5$
 OGD
 - - - - OD
 - · - · - GLRT-LQ

Figure 2.15 P_D against SCR of GLRT-LQ, OGD and OD detectors for perfectly known signal [17]

CHAPTER 3

PROPOSED ALGORITHM

CA CFAR methods are optimum in Gaussian distributed clutter. However, in non-Gaussian distributed clutter, like K-distributed clutter or Weibull distributed clutter, performance of these detectors decreases considerably as they deviate from Gaussian. Moreover these detectors suffer from ghosts. Ghost is a detection that results from target but at a point where there is no target. There are two main sources of ghosts. First one is the pulse compression which produces time sidelobes. If target echo is strong enough, sidelobes appear above noise floor. This may cause false detections, in other words ghosts, at the transition regions of noise level and target side lobes. Doppler spreading is another source of ghosts. Because of the filter response of the Doppler filters, peaks may arise at the output of Doppler processor around target Doppler, which causes ghosts.

In this thesis, a method is proposed in order to improve the performance of CA CFAR. There are two main purposes of this algorithm. First one is reducing false alarms and ghosts that appear after CA CFAR. Second one is keeping the P_D value of original CA CFAR. This method makes use of Doppler spreading behaviors that appear as the result of Doppler processing. Therefore it is called Doppler Pattern Matching.

DPM is tightly related to Doppler Processing method that is used. Therefore, before the description of it, Doppler processing method that is used in analysis will be explained. After that, Doppler spreading concept will be described. Finally, DPM will be explained in details.

3.1 Doppler Processing Method Used in Analysis

In Section 2.2.2, it was stated that $\mathbf{p}^H \mathbf{M}^{-1} \mathbf{z}$ term in the GLRT-LQ detector can be treated as a regular Doppler processor. \mathbf{M}^{-1} transformation applies MTI clutter suppression to signal and \mathbf{p}^H multiplication is the classical DFT Doppler processor. In this thesis, this method is used as Doppler processor. In order to identify the performance of this detector, some studies have been done that compares original MTI followed by DFT with this method which will be demonstrated in Section 3.1.2.

In this study, formation of interference covariance matrix \mathbf{M} has a critical importance. In Section 2.2.2, analysis results were demonstrated that uses matrix \mathbf{M} with the elements $m_{ij} = \rho^{|i-j|}$, ($i, j = 1, 2, \dots, K$) where ρ is the one lag correlation coefficient and K is the number of processed pulse. In [18], [19], [23], [24] also \mathbf{M} is formed in this way. In this thesis, \mathbf{M} is formed in a different fashion.

3.1.1 Obtaining Interference Covariance Matrix

In this thesis, to model radar system from transmitter phase code generator to the pulse compression filter output, discrete time system model that is explained in [12] is used. The block diagram which is discretized at the chip rate is shown in Figure 3.1.

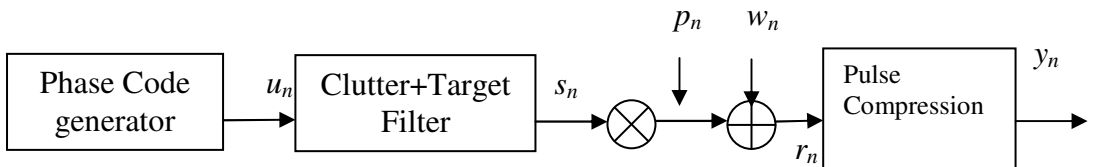


Figure 3.1 Baseband discrete-time equivalent system model[12]

In this model, output of the pulse compression filter can be written as

$$y_n(k) \cong p_n(k) \left[\Psi_0(\omega_d) h_n(k) + NA(k) e^{j\Omega k} \delta_{n-R} \right] + \eta_n(k) \quad 0 \leq k \leq K-1 \quad (3.1)$$

where

$y_n(k)$ is the pulse compression output for the k 'th pulse and n 'th sample of the k 'th observation

$p_n(k)$ is the value of the discrete-time baseband equivalent carrier for the k 'th pulse and n 'th sample of the k 'th observation,

Ψ_n is the autocorrelation of the phase code sequence u_n ,

h_n represents the clutter return process,

N is the number of chips in the pulse,

A denotes the target echo signal amplitude including phase noise,

$\Omega = 2\pi f_0 \left(\frac{2vT_p}{c} \right)$ is the phase accumulation from the target due to its velocity

from a pulse to the next,

$\omega_d = 2\pi \frac{2v_r}{c} \frac{f_0}{R_c}$ is the discrete-time Doppler frequency shift due to target's radial

velocity,

η_n is a white Gaussian sequence with variance $N\sigma^2$.

By dropping the fast index n , Eq (3.2) becomes

$$y(k) \cong p(k) \left[\Psi_0(\omega_d) h(k) + NA(k) e^{j\Omega k} \right] + \eta(k) \quad 0 \leq k \leq K-1 \quad (3.2)$$

According to this model, interference covariance matrix \mathbf{M} is equal to sum of clutter autocorrelation matrix and noise autocorrelation matrix:

$$\mathbf{M} = \mathbf{R}_C + \mathbf{R}_N \quad (3.3)$$

Elements of the noise autocorrelation matrix \mathbf{R}_N is equal to

$$R_N(n, k) = \frac{N_0}{2} \delta_{k-n} \quad (3.4)$$

where N_0 is the power spectral density of noise.

Elements of the clutter autocorrelation matrix \mathbf{R}_C is equal to [5]

$$R_C(n, k) = R_{hm}(n-k)R_d(n-k) \sum_i R_p(n-k; R_1 + (n-i)L) E_c[R_1 + (n-i)L] \quad (3.5)$$

R_{hm} is the is the normalized auto correlation function accounting for antenna scanning modulation with elements

$$R_{hm}(n, k) = \exp(-2 \ln 2 \Delta\phi^2(n, k) / \phi_{BW}^2) \quad (3.6)$$

where ϕ_{BW} is the antenna beam width and $\Delta\phi$ represents the difference of the angle of antenna at pulses n and k[5].

R_p is the matrix formed from the phase noise autocorrelation function where

$$R_p(n-k; T_p) = E\{p(n)p^*(k)\} = \begin{cases} 1 - \sigma_p^2(|(n-k)|T_p) & k \neq n \\ 1 & k = n \end{cases} \quad (3.7)$$

T_p is the chip width. $\sigma_p^2(T)$ is the local oscillator phase variance at time spacing T, and is given by

$$\sigma_p^2(T) = 1 - |R_p(T)|^2, \quad R_p(T) = \int_{-\infty}^{\infty} S_p(f) e^{j2\pi f T} df \quad (3.8)$$

$S_p(f)$ is the PSD of the carrier, which is translated to baseband. Power spectral density must be normalized so that the carrier power is unity, i.e., $R_p(0) = 1$ [13].

L is the number of range bins in a PRI. R_l is equal to modulus of range R after division by L where R is the range bin of the processed cell.

$E_c(r)$ denotes the average energy return from the clutter at range r and is equal to [1]

$$E_c(r) = \frac{E_T G_T G_R \sigma^0 \theta_B \Delta R A_e}{(4\pi)^2 R^3 \cos(\varphi)} \quad (3.9)$$

where E_T denotes the transmitted energy, G_T is transmit gain, G_R is receive gain, σ^0 is the surface back scattering coefficient, ΔR is the range resolution, A_e is the antenna effective aperture, θ_B is the 3dB azimuthal beamwidth and φ is the grazing angle.

3.1.2 Comparison of GLRT-LQ Doppler Processor with MTI-DFT

Performance of GLRT-LQ Doppler processor can be compared with MTI-DFT using their filter responses. In Figure 3.2, response of a single filter for both processors can be observed in a scenario where 8 process pulses are used. Frequency selectivity of MTI-DFT filter is better than GLRT-LQ Doppler filter. However, GLRT-LQ Doppler filter achieves 5 dB more SNR than MTI-DFT filter. This behavior can also be observed from the Figure 3.3, which demonstrates maximum of responses of 8 pulse filter bank both for two types of processors.

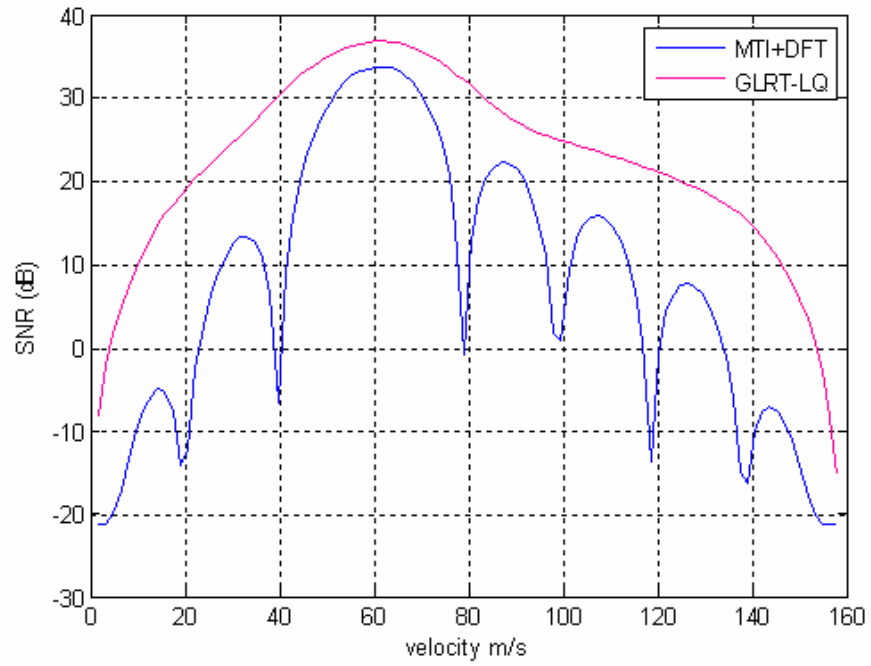


Figure 3.2 Response of one MTI+DFT filter and GLRT-LQ Doppler Filter

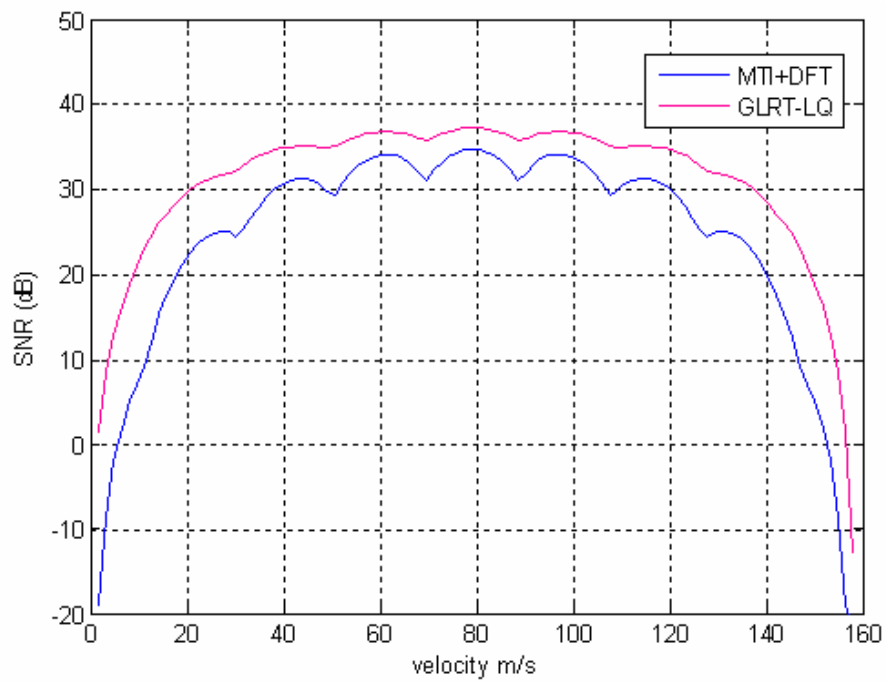


Figure 3.3 Maximum of responses for MTI+DFT and GLRT-LQ Doppler Filter

As a result, GLRT LQ Doppler processor considered being a better Doppler processor and it is used in the analysis of this thesis.

3.2 Doppler Spreading Concept

Target signal spreads on Doppler after Doppler processing. This behavior is also valid for GLRT-LQ Doppler processor. The Doppler vs. range matrix at the output of GLRT-LQ Doppler processor demonstrates this property. In Figure 3.4 there is an example Doppler vs. range matrix, where number of process pulses is 8 and number of range cells in a PRI is 1500. In this matrix, there is a target is on 5th Doppler bin and 1000th range bin. However, peaks can be observed on Doppler bins other than target's Doppler bin.

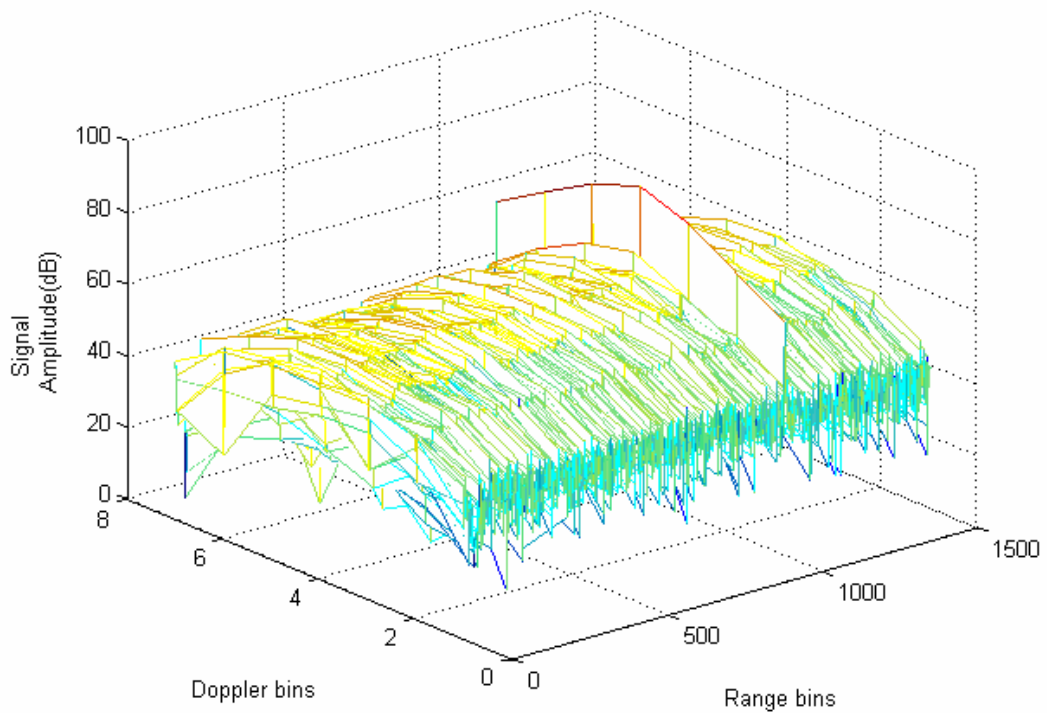


Figure 3.4 An example of 8 pulse 1500 range bin Doppler processing output
Doppler-Range matrix

After investigating Doppler spreading behavior of targets with different Doppler frequencies, it is observed that this behavior is characteristic to Doppler frequency of the target. This can be demonstrated using an example. In a scenario, where 8 processed pulses are used, there are seven main Doppler bins that targets can show up successfully; the signal on first Doppler bin is mainly composed of noise and clutter echoes. Target signals with seven different Doppler frequencies, each matching with a Doppler bin, are produced. These signals are passed through a pulse compression filter, then Doppler processor and finally linear law detector in order to obtain range versus Doppler matrix. Doppler samples at target range cell are taken and vectors with size 8×1 are formed for each Doppler frequency case. These vectors are scaled to set the maximum value in the vector to 1 and plotted in

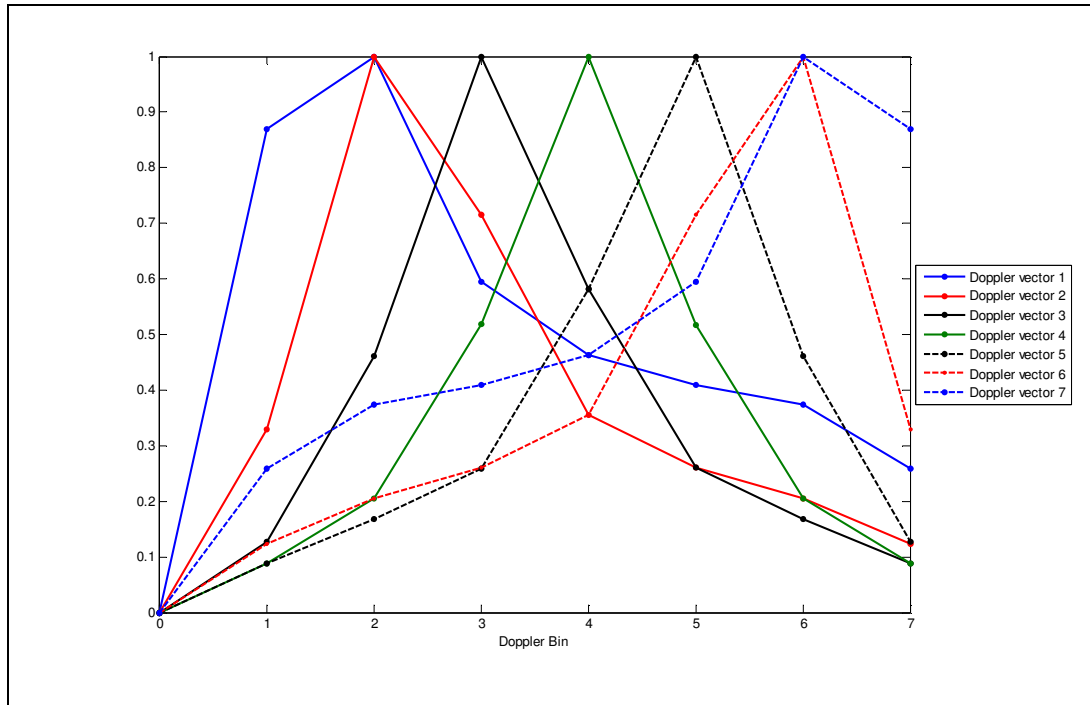


Figure 3.5 Doppler spreading vectors

In Figure 3.5, it can be observed that each Doppler frequency produces patterns with different shapes. In addition to this, patterns produced by target signals will be different than pattern produced by disturbance signal. This is expected since moving target signals have different Doppler characteristics than disturbance signal.

Using Doppler spreading behavior, Doppler patterns are obtained. The function of these Doppler patterns in DPM and the way to obtain these patterns will be described in the following section.

3.3 Description of DPM

Working principle of DPM can basically be gathered from the data flow diagram in Figure 3.6. Main input to DPM block is the detections results of CA CFAR. Doppler-Range matrix at the output of linear law detector and predetermined

Doppler patterns are auxiliary inputs. In the DPM block, some of the detections are eliminated and marked as false alarm. Meanwhile, it is possible for some real detection to be eliminated. As a result, detections that stay after elimination will be obtained.

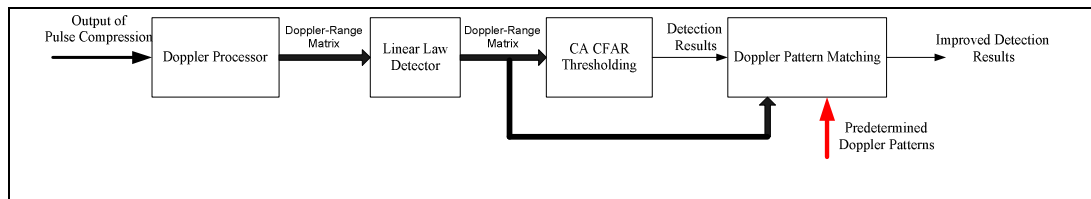


Figure 3.6 Data flow diagram of DPM

Operation steps of DPM are as follows:

1. Range bin, Doppler bin and amplitude of the detections at the output of CA CFAR are passed to DPM block.
2. Doppler bin of the detection determines the Doppler pattern that will be used in matching, among all of the Doppler patterns.
3. The similarity of the Doppler pattern detected at the range cell of interest to the expected Doppler pattern at each Doppler bin is computed. Doppler-Range matrix is used in this step. Elements of the column at detection range bin are necessary to achieve mentioned Doppler pattern matching check. As a result of this step, a numerical value is obtained, which denotes how much the mentioned patterns are different from each other. This value is called difference factor.
4. Finally, the difference factor is compared with a threshold to decide whether CA CFAR detection is actually detection or not. This threshold is a predetermined constant value that denotes the maximum difference factor to decide that detection is a real one. This threshold is called as secondary threshold since it is the second threshold applied to data after CA CFAR threshold.

In the following section, algorithm will be explained in details.

3.3.1 Details of the Algorithm

In Section 3.3.1.1, the way to obtain the Doppler patterns will be explained. In Section 3.3.1.2, the flow of algorithm will be given in details.

3.3.1.1 Obtaining Doppler Patterns

One of the key points of the algorithm is the Doppler patterns that are auxiliary inputs to DPM block. In this chapter, the way to obtain these Doppler patterns will be explained.

There are $M-1$ main Doppler frequencies, excluding the zero Doppler frequency, that a target may have in a scenario where there is M process pulses. To have better explanation, a specific scenario will be handled which is the scenario used in Section 3.2. In this scenario there are 8 process pulses so there are 7 main Doppler frequencies a target may take. For each case, a different Doppler pattern appears at the output of Doppler processor which can be seen in Figure 3.4. Since the zero Doppler filter output will mainly be constituted of clutter and noise and the Doppler contribution to the zero Doppler response of the moving targets will be quite small, the zero Doppler response will not be included in the Doppler pattern. As a result, Doppler patterns of this scenario are formed using last 7 elements whose maximum element is 1. They can be seen in

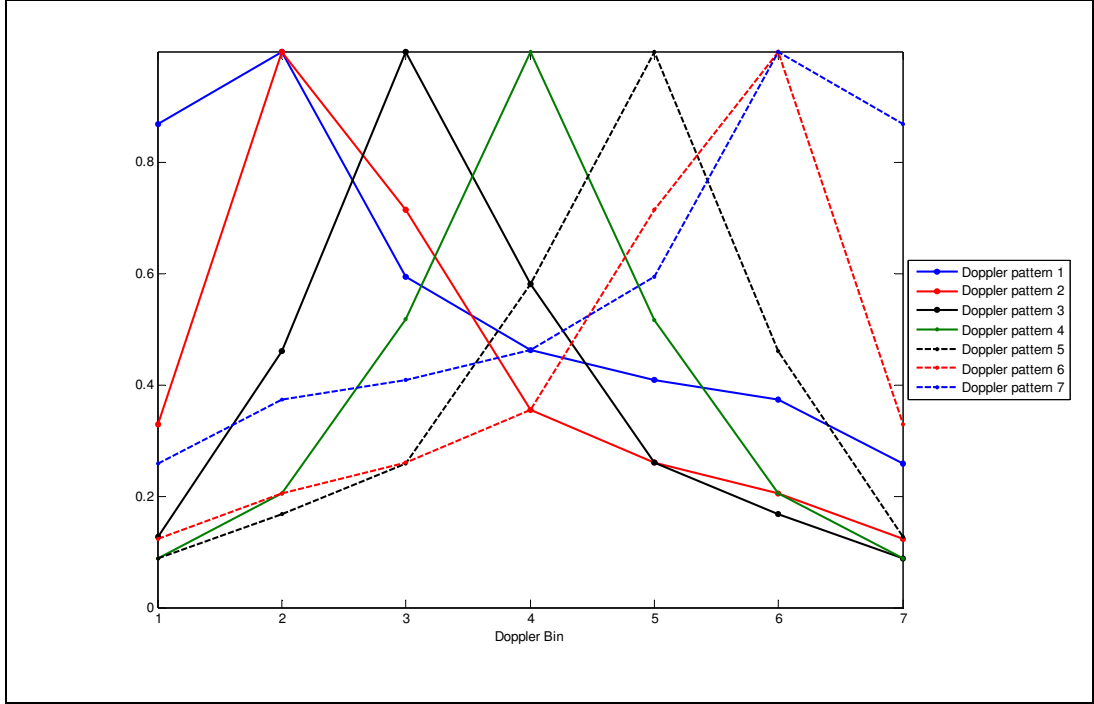


Figure 3.7 Doppler patterns

In a system that uses DPM, there should be a set of Doppler patterns for each set of Doppler filter bank. Each Doppler pattern set will be composed of $M-1$ Doppler patterns, where M is the number of process pulses.

The methodology to form Doppler patterns is given below:

1. Swerling 0 target signal vector s_d is formed for every possible Doppler bin whose components are

$$s_d(i) = 1/\sqrt{M} \times e^{\frac{j2\pi d i}{M}} \quad (3.10)$$

and d is equal to Doppler bin number.

2. Doppler filtering applied to each signal vector and resulting vector for each signal vector with Doppler d is called r_d .
3. First element of r_d that is negligible is taken out from the vector. Remaining elements of the vector are scaled in a way that the maximum value of an element in vector will be 1. Resulting vector is the Doppler pattern corresponding to Doppler d , which is called V_d .

3.3.1.2 Flow of Algorithm

Flow of DPM is given in steps below:

1. Detection result with Doppler bin d , range bin r and signal amplitude level α is passed from CA CFAR block to improvement block.
2. r^{th} column vector of the Doppler-Range matrix at the output of the linear law detector is taken. The first element of this column vector, which is the zero Doppler element, is taken out of this vector and resulting vector is called \mathbf{S} . \mathbf{S} is vector with length $M-1$ where M is the number of processed pulses; d^{th} element of \mathbf{S} is equal to α , $S_d = \alpha$.
3. It can be observed in Figure 3.7 that every Doppler pattern has a triangular shape with a peak point. DPM assumes that CA CFAR detection is detection of a target whose Doppler pattern's peak point is at detection Doppler bin. If it is the case, shapes of vector \mathbf{S} and d^{th} Doppler pattern vector V_d should be alike. The difference of two vectors can give idea of how much they are alike. However, their order of magnitude is different. Maximum value of V_d is 1 whereas the maximum value of \mathbf{S} is α . Therefore, \mathbf{S} should be scaled with $1/\alpha$ in order to have 1 as maximum

value. Resulting vector is called \mathbf{T} and its maximum element is 1.

$$\mathbf{T} = 1/\alpha \times \mathbf{S} \quad (3.11)$$

4. Difference vector of the vectors \mathbf{T} and V_d is calculated and then the absolute value of the elements of \mathbf{Y} is summed up. In other words, \mathcal{L}_1 norm is used. It is possible to use higher order norms.

$$Y = T - V_d \quad (3.12)$$

$$\delta = \sum_1^{M-1} |Y_i| \quad (3.13)$$

The resulting value δ is, in a way, numerical expression of how much the shape of d^{th} Doppler pattern is different from the shape of Doppler pattern at detection range cell r , which was called difference factor in Section 3.3.

However, there are cases where more than one pattern may have Doppler bin d as peak point. In this case δ value will be calculated for all of these patterns.

$$Y_k = T - V_{d(k)}; \quad k = 1, 2, \dots, n \quad (3.14)$$

$$\delta_k = \sum_1^{M-1} |Y_{k,i}| \quad (3.15)$$

where $V_{d(k)}$ denotes the k^{th} Doppler pattern whose maximum element is on Doppler bin d and n is the number of patterns whose maximum element on Doppler bin d .

Minimum of the δ_k values will be chosen to use in the next step:

$$\delta = \min(\delta_1, \delta_2, \dots, \delta_n) \quad (3.16)$$

Furthermore, there are cases where a Doppler bin is not a peak point for any Doppler pattern. In this case, it is tried to match the Doppler patterns of adjacent Doppler bins. δ value is calculated for adjacent Doppler patterns and smaller of them is chosen to be used in next step.

$$\delta = \min(\delta_1, \delta_2) \quad (3.17)$$

5. Final step is comparing δ with a predetermined threshold value η . η is secondary threshold value that was mentioned in Section 3.3. If δ is less than η , then it will be decided that there is a target with Doppler frequency corresponding to Doppler bin d at range cell r . In other case, this would mean that the shape of d^{th} Doppler pattern is different from the shape of Doppler pattern. Therefore CA CFAR detection will be canceled.

$$\begin{array}{c} H_0 \\ \delta > \eta \\ < \\ H_1 \end{array} \quad (3.18)$$

It is obvious that as threshold value η increases, P_D decreases and P_{FA} increases. There is not a closed form expression that relates η to P_D and P_{FA} . Therefore Monte-Carlo simulations are done to determine η to be used in analysis.

3.4 Comments on Proposed Algorithm

Doppler pattern searching is expected to improve CA CFAR by eliminating false detections produced by

- ghosts
- clutter edges

If there is a target, signal will spread on Doppler at target range cell. At target range cell, it is highly probable that more than one detection will occur at target range cell which are called ghost. DPM will question if detection's Doppler bin matches appropriate Doppler pattern. If SNR is high enough, only the appropriate Doppler pattern will match and ghosts will be eliminated.

In case of a false alarm occurs because of clutter edges, DPM will check if the pattern of detection Doppler matches with the pattern on the detection range cell. Patterns will not match with a high probability. As a result, this kind of false alarms will be eliminated.

Although it is advantageous to use DPM in two cases explained above, there is not any use of this method in cases where ghost occur because of sidelobes of pulse compression autocorrelation function, especially if SNR is high. This is because; sidelobes' Doppler frequency is almost equal to target's Doppler frequency.

One can benefit from mentioned DPM to prevent target masking which is a drawback of CA CFAR. For this purpose, SOCA CFAR method was proposed. However, in this case SOCA CFAR suffers from high P_{FA} . DPM can be used as an improvement method for SOCA to prevent P_{FA} from increasing. This approach can be useful for CA CFAR and GOCA CFAR too. CA CFAR's or GOCA CFAR's threshold can be reduced enough to resolve two targets for a required scenario. Then DPM can be used to reduce the number of false alarms.

CHAPTER 4

SIMULATIONS

In order to investigate the performance of DPM, Monte-Carlo Simulation Method is used since it is not possible to obtain an analytical formula of P_D and P_{FD} . In Section 4.1, the method that is used to obtain simulation data will be explained. In Section 4.2 simulation results are shown, which compare original CA CFAR detector with CA CFAR detector after applying DPM. Moreover, results are also compared with OS CFAR which is considered to be successful in the cases where CA CFAR fails.

4.1 Simulation Information

Monte-Carlo simulations are carried out in MATLAB environment. Necessary simulation data is the input data to the pulse compression block. Once the input signal to the pulse compression block is obtained, it is easy to produce the output. Input data to pulse compression block is obtained using Radar Data Simulator in [27]. This tool will be explained in Section 4.1.1.

In this thesis, 100.000 data sets are used in simulations. This number is enough to have accurate results. Moreover, data sets above this number are very hard to achieve with today's computers in a reasonable time.

4.1.1 Radar Data Simulator

Radar Simulator is a very powerful tool, since almost every parameter of signal can be adjusted according to desired scenario. Monte-Carlo simulations are carried out with the following data parameters:

- Transmit power is set to 5000W.
- Radar operating band is X band.
- Number of pulses is set to 10. Eight of pulses are used as processed pulse and 2 pulses are used as fill pulse.
- Pulse Repetition Frequency (PRF) is set to 10 kHz. In this case maximum unambiguous range is :

$$R_{\max} = c / (2 \times PRF) = 3e^8 / (2 \times 1e^4) = 10 \text{ km}$$

and radial velocity corresponding to this PRF is:

$$V_D = \frac{c * PRF}{2 * f_T} = \frac{3e^8 * 1e^4}{2 * 9.5e^9} \cong 157.9 \text{ m/s}$$

- Chip width is set to 66.67 ns. Therefore range resolution is 10 m. Moreover, with the used PRF value, there are 1500 range bins in each Pulse Repetition Interval (PRI).
- System noise figure is set to 3.5 dB.
- Two way loss is set to 2 dB.

- Azimuth beam width is set to 2 degrees and elevation beam width is set to 3 degrees.
- Grazing angle is set to zero degrees.
- Clutter parameters:
 - Clutter is modeled as Weibull distributed with shape parameter set to 0.8.
 - Clutter cross section per unit area, namely σ^0 is set to -20.
- Radar antenna rotation rate is set to 30 revolution per minute (rpm).
- Several terrain shapes can be chosen in this simulator in order to produce clutter signal. In this thesis Babadağ terrain is used, whose shape is plotted in

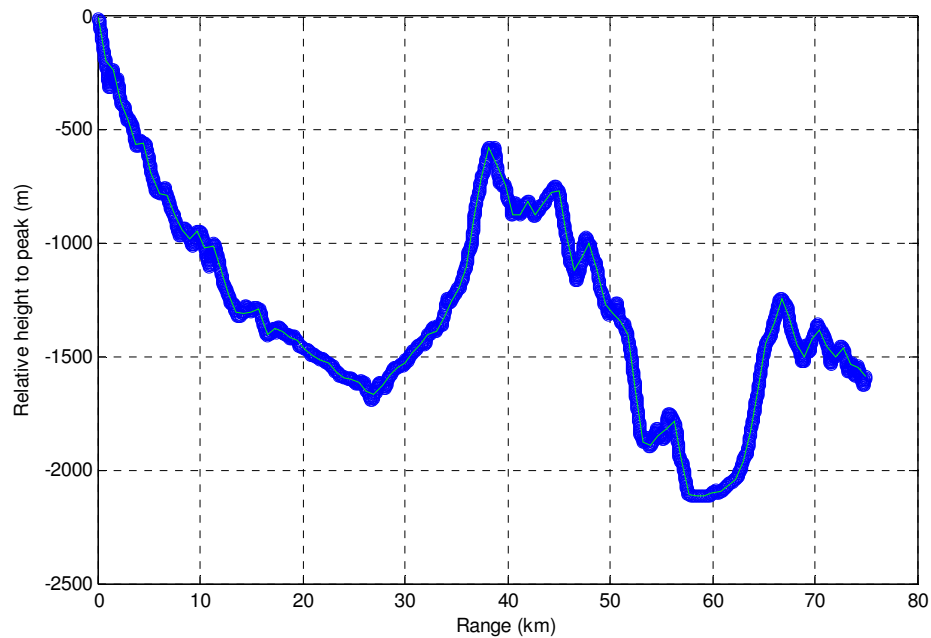


Figure 4.1 Shape of Babadağ Terrain

4.1.2 Processing Parameters

There are three main processing blocks before applying DPM, which are Pulse Compression, Doppler Processing, Linear Law Detector and CA CFAR block. There are some parameters that should be adjusted in these blocks. They are given below:

- A binary phase, length 32 pulse compression code that is published in [7] is used:

[1,1,1, 1,1,1,1,-1,-1,-1,-1,1,1,-1,1,-1,-1,1,-1,1,-1,-1,1,-1,-1,1,1,-1,-1,1,1]

Its ISL is -8.95 dB and PSL is -20.56 dB. Autocorrelation of this code can be seen in

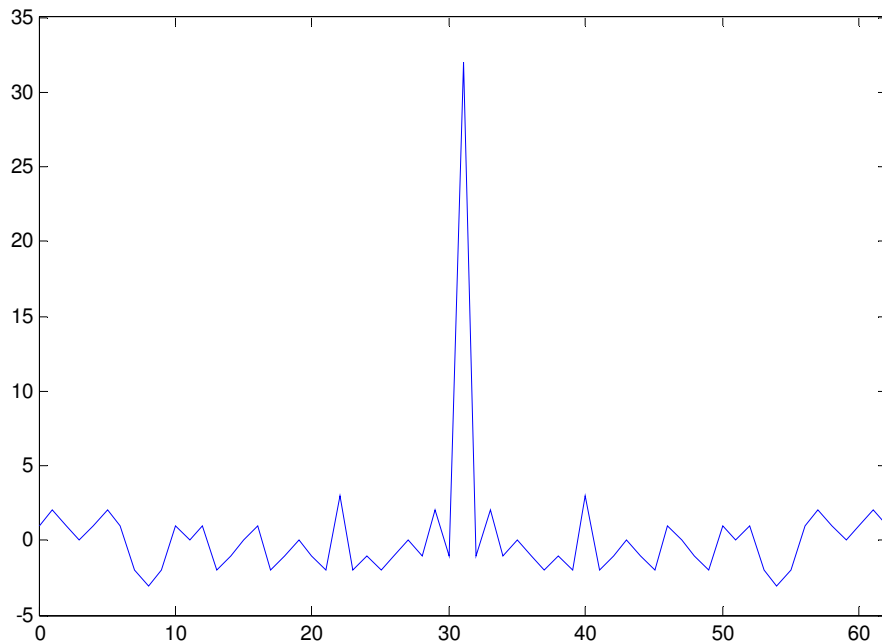


Figure 4.2 Autocorrelation function of pulse compression code that is used

- Scale factor of threshold is set the same for all types of CFAR processors:

$$\alpha = \alpha_{CA} = \alpha_{GOCA} = \alpha_{SOCA} = \alpha_{OS} = 13 \text{ dB}$$

This value is adjusted iteratively by Monte Carlo simulations since there is not a simple closed form equation for obtaining P_{FA} or P_D for the Weibull distributed clutter.

- It is decided to equate threshold η to 1 with some preliminary simulation results.

4.2 Simulation Results

In order to evaluate the performance of DPM, new definitions are made. First one is “Number of False Detections” which is the sum of false alarms and ghost. Related to this definition, “Probability of False Detections”, P_{FD} , is defined, which is equal to sum of probability of ghost (P_G) and P_{FA} . Final definition is the “Improvement Factor” which is a criterion to evaluate the performance. It is calculated as

$$\text{Improvement Factor} = \frac{(\text{Number of false detections of original CA CFAR})}{(\text{Number of false detections of improved CA CFAR})} \quad (4.1)$$

There are three main types of simulations that are carried out. In the first one, a scenario without target is used. Purpose of this simulation is to observe the change in P_{FA} . In second type of simulation, a scenario with a single target is used. In this simulation, change of performance with respect to Doppler and range is observed. These results are also compared with OS CFAR results. In final simulations, a scenario with two targets is used in order to observe target masking behaviors.

4.2.1 Simulations without Target

This type of simulations is carried out to observe the change in P_{FA} . Results of CA CFAR, SOCA CFAR and GOCA CFAR can be observed in Table 4.1. OS CFAR result is also obtained for comparison.

Table 4.1 Simulation result of the scenario without target

Type of Detector	P_{FA} of Original CFAR	P_{FA} of Improved CFAR	Improvement Factor
SOCA	1.27e-4	2.51e-05	5,08
GOCA	4.27e-07	6.76e-08	6,30
CA	1.63e-06	3.54e-07	4,61
OS CFAR	1.23e-07		

P_{FA} values are calculated using 100.000 data sets. There are 10.500 data in each set. Totally, there are 1.05×10^9 data samples. Assuming that each of these data sets is equally probable overall P_{FA} is calculated by averaging P_{FA} of each data set.

Considering the original detectors, OS CFAR is the one that achieves the lowest P_{FA} . However, considering all of the results, improved GOCA CFAR is the best. Improvement factors are close to each other. P_{FA} of every detector is decreased around five times.

4.2.2 Simulations with Single Target

Two types of simulations are carried out in order to analyze the change in P_{FD} and P_D in single target case. In first case, dependency on range is analyzed. In second

case, dependency on Doppler frequency is analyzed.

4.2.2.1 Range Analysis

Target parameters that are kept constant in the simulations are:

- Velocity: 78.95 m/s, 4th Doppler bin
- Radar Cross Section : 3 m²
- Swerling type: 0

Target's range is varied from 10km to 40 km.

4.2.2.1.1 CA CFAR Range Analysis

CA CFAR simulation results are given in Table 4.2.

Table 4.2 CA CFAR simulation result of the scenario with a single target*

Range(km)	10	13.3	16.67	20	23.3	26.67	33.3	36.67	40
SNR(dB)	26.51	26.41	26.23	25.89	25.36	24.71	22.98	21.98	20.91
P_D	1	1	1	1	1	1	1	1	1
Average Number of False Detections per beam of original CA CFAR	6.016	6.017	6.017	6.017	6.018	6.016	6.016	6.014	5.914
Average Number of False Detections per beam of CA CFAR after DPM	0.0034	0.0036	0.0034	0.0036	0.004	0.0034	0.0032	0.0039	0.0036
P_{FD} of original CA CFAR	5.73×10^{-4}	5.73×10^{-4}	5.73×10^{-4}	5.73×10^{-4}	5.73×10^{-4}	5.73×10^{-4}	5.73×10^{-4}	5.73×10^{-4}	5.63×10^{-4}
P_{FD} of CA CFAR after DPM	3.19×10^{-7}	3.45×10^{-7}	3.28×10^{-7}	3.44×10^{-7}	3.78×10^{-7}	3.24×10^{-7}	3.07×10^{-7}	3.75×10^{-7}	3.45×10^{-7}
Improvement Factor	1796	1662	1749	1667	1516	1770	1868	1526	1634

*In this table P_D and P_{FD} values are detection rates and false detection rates respectively obtained at the result of simulations.

P_D is 1 both for improved CFAR and original CFAR. However, there is a huge difference in the number of false detections. Considering the original CA-CFAR, there is six plus a little percentage of false detections for each beam. Six false alarms are in fact ghosts; remaining percentage part stands for the false alarms that result from clutter and noise. However, it can be observed from the results that ghosts are eliminated by DPM and P_{FD} reduces to $3e^{-7}$ which is a value close to P_{FA} of CA CFAR after DPM in Table 4.1. Moreover, Improvement Factor gives an idea about reduction in P_{FD} . Number of false detections is reduced 1526 times at worst case and 1868 at best case.

In order to make a fair comparison, threshold scale factor of CA CFAR, α_{CA} , is adjusted for each range value so that number of false alarms plus number of ghosts are set almost to number of false detections in the improved CA CFAR case; and P_D is investigated. The result of this simulation can be seen in

Table 4.3 Simulation result of the scenario with a single target

Range(km)	10	13.3	16.67	20	23.3	26.67	33.3	36.67	40
P_D	0.002	0.005	0.022	0.060	0.169	0.307	0.578	0.673	0.614
Number of false detections per beam	0.004	0.003	0.004	0.004	0.004	0.003	0.004	0.005	0.003

P_D values are smaller than the ones in Table 4.2. The largest value 0.6 is not a tolerable value. In Table 4.3, P_D decreases as the range increases. Originally, reverse of it is expected since SNR decreases as the range increases. However, in this case it is normal because number of ghosts increases as the SNR increases since target signal is the source of ghost. Keeping P_{FD} constant will make P_D decrease as the range increases.

4.2.2.1.2 SOCA CFAR Range Analysis

Result of range analysis of SOCA CFAR is given in Table 4.4 P_{FD} is very large both for original SOCA CFAR and improved SOCA CFAR when compared to CA CFAR results. Moreover, Improvement Factor is much smaller than CA CFAR's Improvement Factor. The smallest P_{FD} achieved is approximately $2.5e^{-5}$ which is almost 100 times larger than CA CFAR's P_{FD} . Even though it is a tolerable value, for close targets P_{FD} value reaches $1e^{-3}$, which is not useful. As a result, it can be said that DPM is not successful for SOCA CFAR and small Improvement Factor is the proof of it.

Table 4.4 SOCA CFAR simulation result of the scenario with a single target*

Range(km)	10	13.3	16.67	20	23.3	26.67	33.3	36.67	40
SNR(dB)	26.51	26.41	26.23	25.89	25.36	24.71	22.98	21.98	20.91
P_D	1	1	1	1	1	1	1	1	1
Average Number of False Detections per beam of original SOCA CFAR	50.697	22.378	11.468	8.252	7.518	7.386	7.342	7.338	7.288
Average Number of False Detections per beam SOCA CFAR after DPM	10.804	6.635	3079.000	0.962	0.399	0.299	0.266	0.265	0.264
P_{FD} of original SOCA CFAR	4.83x10 ⁻³	2.13x10 ⁻³	1.09x10 ⁻³	7.86x10 ⁻⁴	7.16x10 ⁻⁴	7.03x10 ⁻⁴	6.99x10 ⁻⁴	6.99x10 ⁻⁴	6.94x10 ⁻⁴
P_{FD} of SOCA CFAR after DPM	1.03x10 ⁻³	6.32x10 ⁻⁴	2.93x10 ⁻⁴	9.16x10 ⁻⁵	3.80x10 ⁻⁵	2.85x10 ⁻⁵	2.53x10 ⁻⁵	2.52x10 ⁻⁵	2.51x10 ⁻⁵
Improvement Factor	5	3	4	9	19	25	28	28	28

*In this table P_D and P_{FD} values are detection rates and false detection rates respectively obtained at the result of simulations.

4.2.2.1.3 GOCA CFAR Range Analysis

Result of range analysis of GOCA CFAR is given in Table 4.5. P_{FD} value of original GOCA CFAR is close to original CA CFAR's P_{FD} value. On the other hand, P_{FD} value of improved GOCA CFAR is approximately six times better than improved CA CFAR's P_{FD} value on the average. P_{FD} is $4e^{-8}$ at best case and $8e^{-8}$ at worst case which are successful results with a P_D of 1. Likewise, Improvement Factor is 6 times better compared to CA CFAR. As a result, DPM's performance is better than its performance in CA CFAR, even the best in all three cell averaging type CFAR detectors when there is a single target.

Table 4.5 GOCA CFAR simulation result of the scenario with a single target*

Range(km)	10	13.3	16.67	20	23.3	26.67	33.3	36.67	40
SNR(dB)	26.51	26.41	26.23	25.89	25.36	24.71	22.98	21.98	20,91
P_d	1	1	1	1	1	1	1	1	1
Average Number of False Detections per beam of original GOCA CFAR	6.004	6.004	6.004	6.004	6.004	6.004	6.005	5.993	5.753
Average Number of False Detections per beam GOCA CFAR after DPM	0.000	0.001	0.001	0.001	0.001	0.001	0.001	0.001	0.001
P_{FD} of original GOCA CFAR	5.72x10 ⁻⁴	5.72x10 ⁻⁴	5.72x10 ⁻⁴	5.72x10 ⁻⁴	5.72x10 ⁻⁴	5.72x10 ⁻⁴	5.72x10 ⁻⁴	5.71x10 ⁻⁴	5.48x10 ⁻⁴
P_{FD} of GOCA CFAR after DPM	4.00x10 ⁻⁸	6.76x10 ⁻⁸	5.33x10 ⁻⁸	6.76x10 ⁻⁸	6.76x10 ⁻⁸	6.10x10 ⁻⁸	6.76x10 ⁻⁸	8.00x10 ⁻⁸	5.81x10 ⁻⁸
Improvement Factor	14295	8457	10721	8457	8457	9382	8457	7134	9431

*In this table P_D and P_{FD} values are detection rates and false detection rates respectively obtained at the result of simulations.

4.2.2.1.4 OS CFAR Range Analysis

Range analysis result of OS CFAR is given in Table 4.6 in order to compare with the improved cell averaging type CFAR detectors. OS CFAR also suffers from ghosts for higher SNR cases, as can be understood from P_{FD} . After range of 33.3 km, P_{FD} decreases significantly. However, P_D decreases drastically with decreasing P_{FD} ; it is almost impossible to detect targets. Therefore, it can be said that for OS CFAR cannot compete with improved detectors especially for low SNR cases.

Table 4.6 OS CFAR simulation result of the scenario with a single target*

Range(km)	10	13.3	16.67	20	23.3	26.67	33.3	36.67	40
SNR(dB)	26.51	26.41	26.23	25.89	25.36	24.71	22.98	21.98	20.91
P_D	1	1	1	1	0.995	0.823	0.11	2.63x10 ⁻²	8.27x10 ⁻³
Average Number of False Detections per beam	6.01	6.00	5.81	3.33	1.25	0.288	1.70x10 ⁻²	7.16x10 ⁻³	5.60x10 ⁻³
P_{FD}	5.72x10 ⁻⁴	5.72x10 ⁻⁴	5.54x10 ⁻⁴	3.17x10 ⁻⁴	1.19x10 ⁻⁴	2.74x10 ⁻⁵	1.62x10 ⁻⁶	6.82x10 ⁻⁷	5.33x10 ⁻⁷

*In this table P_D and P_{FD} values are detection rates and false detection rates respectively obtained at the result of simulations.

P_D results of the analysis are given in Figure 4.4 and Figure 4.5. In these figures, Doppler frequencies of target do not perfectly match with Doppler bins. These Doppler frequencies fall between two adjacent Doppler bins. Therefore, two different P_D values are demonstrated. Figure 4.4 demonstrates P_D values at Doppler bin that is close to target frequency and Figure 4.5 demonstrates P_D values at Doppler bin that is far to target frequency.

Considering original CA CFAR, P_D values are close to 1 at almost every Doppler frequency both for nearby Doppler bin and far Doppler bin. After DPM, P_D values at close Doppler bin decreases considerably for some Doppler frequencies whereas it stays the same for most of the Doppler frequencies. The Doppler frequencies where P_D decreases are those that are close to zero Doppler. On the other hand, P_D values at far Doppler bin decreases considerably at almost every Doppler frequency. As a result, it can be said that DPM chooses the close Doppler bin for most of the Doppler frequencies.

By looking at the Figure 4.4, it can be observed that most of the Doppler frequencies where P_D decreases are those that are close to zero Doppler. Other than those, there are three Doppler frequencies where P_D decreases. Doppler bin numbers corresponding to these Doppler frequencies are 2.40, 4.50 and 5.67. By looking at the Figure 4.5, another property of these frequencies can be extracted. P_D of far Doppler bin at these frequencies do not decrease considerably. At these Doppler frequencies DPM fails in choosing the close Doppler bin, it chooses the far Doppler bin. This is because; these Doppler frequencies are close to the middle of two Doppler bins. On the other hand, same kind of behavior can be observed for the Doppler frequencies around the middle of 3rd and 4th Doppler bin can be observed. DPM achieves high P_D at close Doppler bin. However, P_D at far Doppler bin is not small enough.

Overall behavior of change in P_D can be summarized as follows:

- P_D decreases considerably after DPM for those frequencies close to zero Doppler frequencies, both for close Doppler bin and far Doppler bin.
- DPM chooses close Doppler bin as the target's Doppler bin for those Doppler frequencies that exactly matches with Doppler bins.
- DPM fails in choosing close Doppler bin as the target's Doppler bin for those Doppler frequencies close to Doppler frequencies that are close to middle of Doppler bins. It may choose the far Doppler bin as the Doppler bin of the target's Doppler frequency.

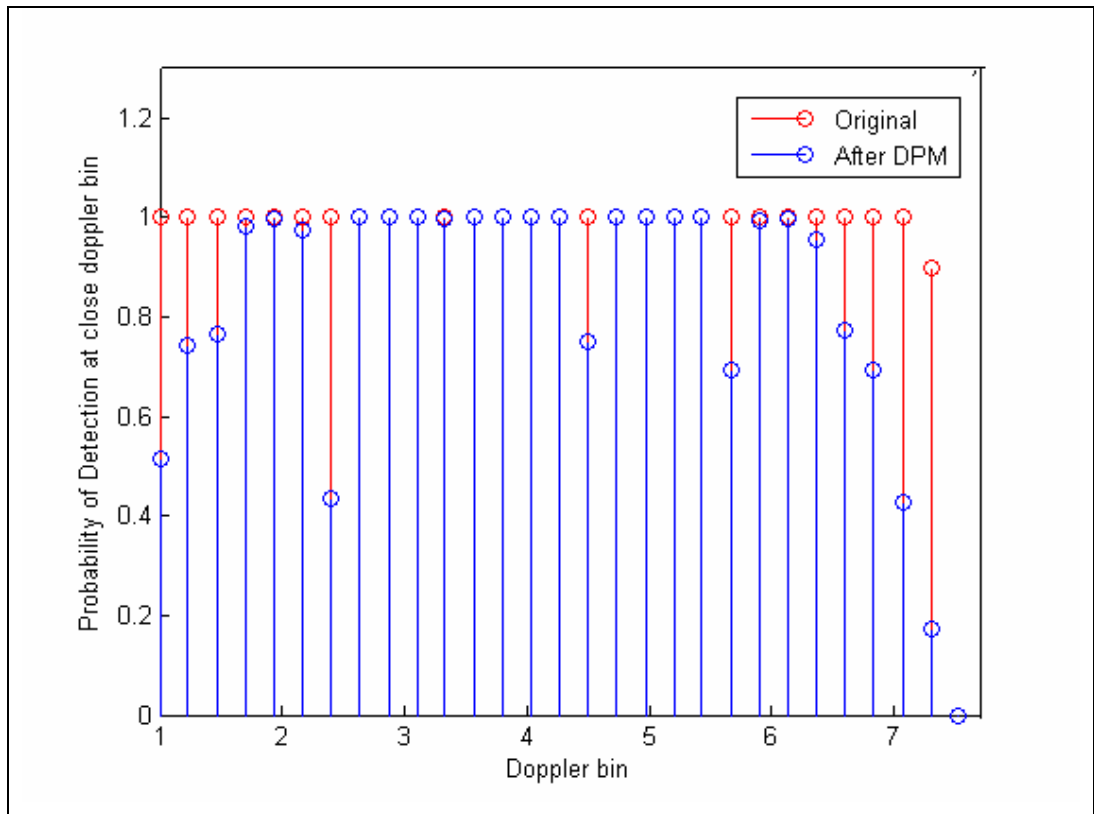


Figure 4.4 P_D values at close Doppler bin

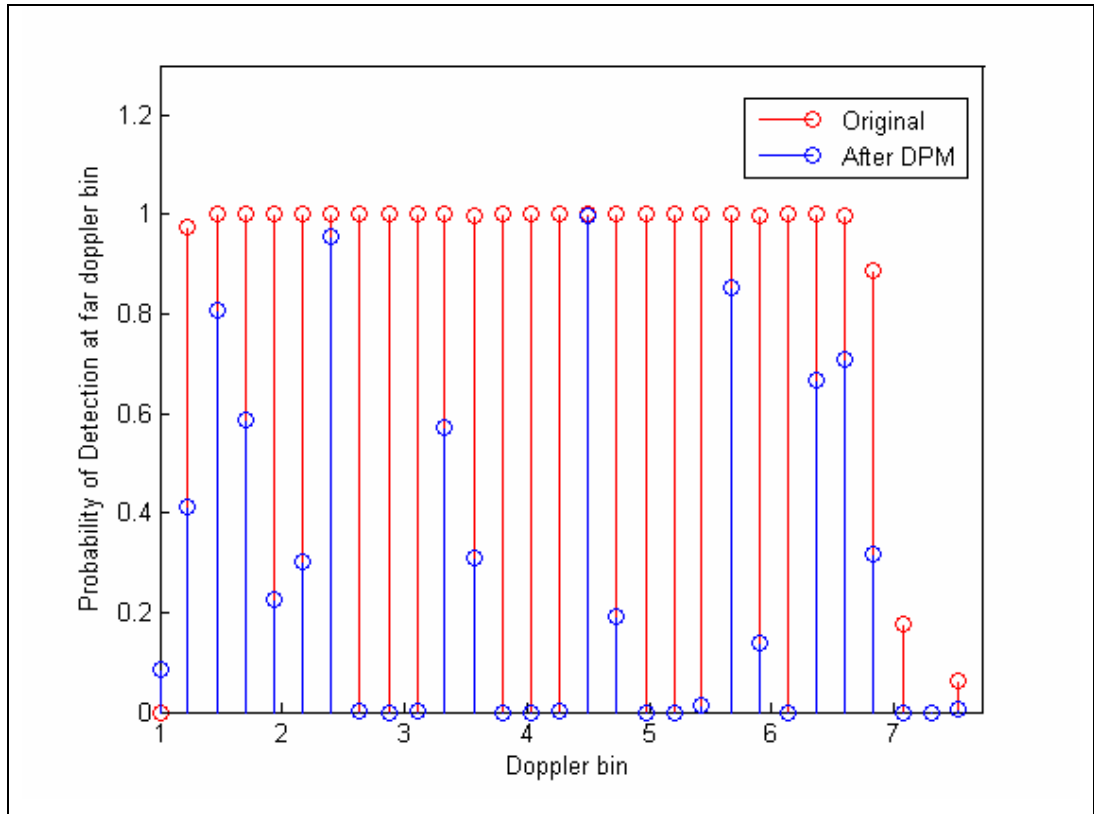


Figure 4.5 P_D values at far Doppler bin before and after DPM

P_{FD} results of the analysis can be observed in Figure 4.6 and Figure 4.7. For most of the frequencies, DPM achieves reducing P_{FD} and making it almost equal to P_{FA} of CFAR after DPM found in Section 4.2.1. For a few Doppler frequencies, DPM has poor performance compared to other Doppler frequencies. Overall P_{FD} performance of DPM can be observed in Figure 4.7. For the 90 percent of Doppler frequencies, DPM achieves 10^2 and more improvement in P_{FD} . For the 52 percent of Doppler frequencies, DPM achieves 10^3 and more improvement in P_{FD} . As a result, DPM has a good performance in reducing P_{FD} .

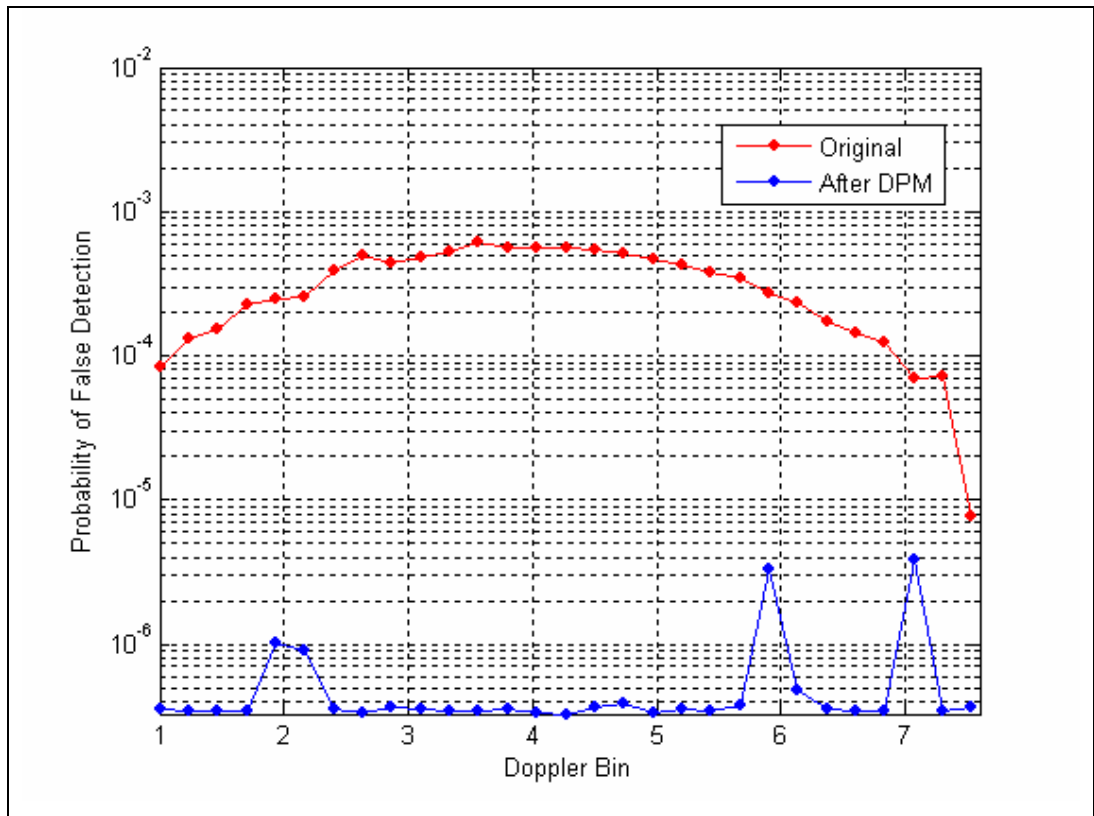


Figure 4.6 P_{FD} values before and after DPM

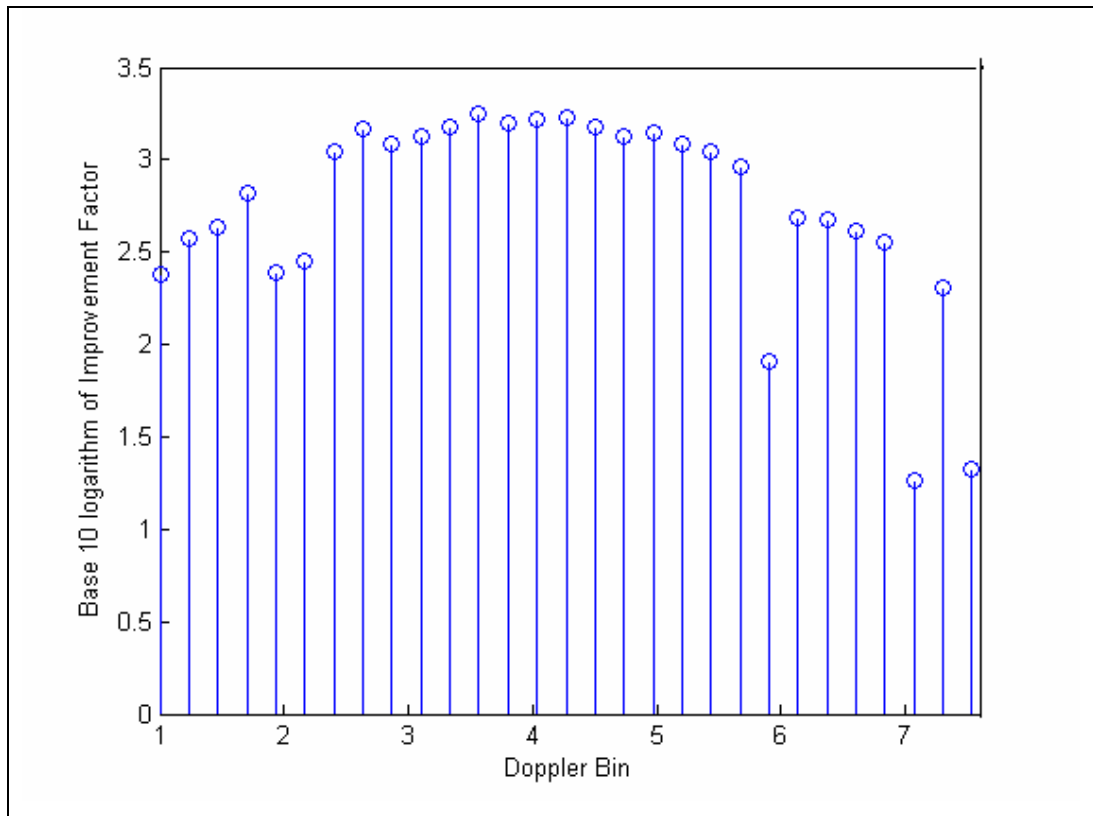


Figure 4.7 Base 10 logarithm of Improvement Factor

4.2.3 Simulations with Two Targets

Several two target scenarios have been handled in order to understand how the DPM affects the target masking properties of cell averaging type of filters. In these simulations, CA CFAR and GOCA CFAR analysis are done. SOCA CFAR analyses are not done because it has been shown that the DPM could not be successful in SOCA CFAR. Moreover, OS CFAR analyses are also not done. This is because; in the simulations scenarios targets are around 40 km in range and OS CFAR fails in detecting target at this range as it is shown in Section 4.2.2.1.4.

4.2.3.1 Scenario 1

Properties of the targets in the simulations are given in Table 4.7. In this scenario, there are two targets that are close in range and have the same SNR value and Doppler frequency.

Table 4.7 Properties of target in the Scenario 1

	Target 1	Target 2
Range(km)	39.96	40
Radial Velocity(m/s)	78.95	78.95
Accurate Doppler bin	4	4
SNR (dB)	20.95	20.91

Results of the simulations are given in Table 4.8. Both improved CA CFAR and GOCA CFAR achieves P_D of 1 which means that there is no reduction in P_D after applying DPM to these detectors. On the other hand, change in the P_{FD} value is different for two detectors. P_{FD} of GOCA CFAR is approximately six times smaller than CA CFAR's P_{FD} . Therefore, one can say that it is advantageous to apply DPM to GOCA CFAR in the cases where there are two targets with same SNR, same Doppler and close range.

Table 4.8 Simulation results of Scenario 1*

	CA	GOCA
P_D of target 1	1	1
P_D of target 2	1	1
P_{FD} before DPM	1.13x10 ⁻³	9.43x10 ⁻⁴
P_{FD} after DPM	3.70x10 ⁻⁷	5.81x10 ⁻⁸
Improvement Factor	3041	16300

*In this table P_D and P_{FD} values are detection rates and false detection rates respectively obtained at the result of simulations.

4.2.3.2 Scenario 2

Properties of the targets in the simulations are given in Table 4.9. In this scenario there are two targets that are very close in range, close in Doppler. Their SNR value is almost the same.

Table 4.9 Properties of target in the Scenario 2

	Target 1	Target 2
Range(km)	39.96	40
Radial Velocity(m/s)	78.95	86.85
Accurate Doppler bin	4	4.5
SNR (dB)	20.91	19.93

*In this table P_D and P_{FD} values are detection rates and false detection rates respectively obtained at the result of simulations.

Results of the simulation are given in Table 4.10. P_D of both two targets for the original CA CFAR and GOCA CFAR is equal to 1. P_D of first target is equal to 1 for the improved detector too. However P_D of the second target reduces to 0.99774; this is still a high probability of detection. Since the second target's Doppler frequency does not match with a Doppler bin, it shows up at two Doppler bins. For the original detectors P_D of second target at second Doppler bin is equal to 1. It reduces to 0.75383 after applying. Reduction in P_D is a considerable amount in this case. Since P_D of this target at other Doppler bin is high enough, this is not a problem that will prevent the target to be detected. On the other hand, improvement in P_{FD} is pretty good when compared to reduction in P_D . For the CA CFAR, improvement factor is equal to 283. It is even better for GOCA CFAR, which is equal to 1196. As a result, it can be said that it is advantageous to use DPM in GOCA CFAR since it keeps P_D high enough with the smallest P_{FD} .

Table 4.10 Simulation results of Scenario 2*

	CA	GOCA
P_D of target 1 before DPM	1	1
P_D of target 1 after DPM	1	1
P_D of target 2 at 4. Doppler bin before DPM	1	1
P_D of target 2 at 4. Doppler bin after DPM	0.99774	0.99774
P_D of target 2 at 5. Doppler bin before DPM	0.99221	0.94468
P_D of target 2 at 5. Doppler bin after DPM	0.75383	0.75383
P_{FD} before DPM	1.08x10 ⁻⁴	9.00x10 ⁻⁵
P_{FD} after	3.82x10 ⁻⁷	7.52x10 ⁻⁸
Improvement Factor	283	1197

*In this table P_D and P_{FD} values are detection rates and false detection rates respectively obtained at the result of simulations.

4.2.3.3 Scenario 3

Properties of the targets in the simulation are given in Table 4.11. In this scenario, there are two targets in scenario that are close in range. There is 8.5 dB difference in their SNR and they are on adjacent Doppler bins.

Table 4.11 Properties of target in the Scenario 3

	Target 1	Target 2
Range(km)	39.96	40
Radial Velocity(m/s)	78.95	86.85
Accurate Doppler bin	5	4
SNR (dB)	25.51	17.07

Results of the simulation are given in Table 4.12. P_D of target-1 stays the same both for two types of detectors, after DPM is applied. However, P_D of target-2 is different for CA CFAR and GOCA CFAR after DPM. P_D CA CFAR is an acceptable value while P_D GOCA CFAR is not. Therefore, it can be said that DPM fails in GOCA CFAR detectors in the cases where there are two targets with different SNR. On the other hand, it is appropriate to use DPM in CA CFAR in such cases.

Table 4.12 Simulation results of Scenario 3*

	CA	GOCA
P_D of target 1 before DPM	1	1
P_D of target 1 after DPM	1	1
P_D of target 2 before DPM	0.97694	0.76217
P_D of target 2 after DPM	0.97694	0.76217
P_{FD} before DPM	0.000718	0.000662
P_{FD} after DPM	3.96×10^{-6}	3.67×10^{-6}
Improvement Factor	1813	1802

*In this table P_D and P_{FD} values are detection rates and false detection rates respectively obtained at the result of simulations.

CHAPTER 5

CONCLUSIONS

In this thesis, an improvement method for CA CFAR is proposed. The aim of this method is reducing false alarm rate while keeping the value of probability of detection. This method makes use of Doppler spreading behaviors that appear after Doppler processing. It tries to match the Doppler spreading pattern of CA CFAR detections to the appropriate predetermined Doppler spreading patterns. If successful pattern matching occurs, then CA CFAR detection is approved. On the other hand, if a pattern matching cannot be achieved, then CA CFAR detection is eliminated. Therefore, this method is called Doppler Pattern Matching.

In this thesis, a new definition is made which is “probability of false detection”, P_{FD} . It equals to sum of P_{FA} and P_G where P_G denotes “probability of ghost”. Ghost is a detection resulting from target energy at a point where there is no target. There are two main sources of ghost. First one is pulse compression. Second one is the Doppler spreading of target signal at the output of Doppler processing block. Doppler pattern matching method is expected to eliminate the ghosts produced by Doppler spreading. However, it is not expected that it will eliminate ghosts resulting from pulse compression.

In order to analyze the performance of the algorithm, Monte-Carlo simulations are carried out. 10^5 data sets are used in each simulation to have valid results. In order to produce simulation data, Radar Data Simulator given in reference [27] is used.

In these simulations, a criterion called improvement factor is defined to evaluate the performance of DPM. It is equal to the ratio of the original P_{FD} to the P_{FD} after

applying DPM. Three types of simulations are carried out; Simulations without target, simulations with single target and simulations with two targets.

Simulations without target are done to observe only the change in P_{FA} since there is no ghost without target. Doppler pattern matching method is applied to CA CFAR, SOCA CFAR and GOCA CFAR. Moreover, OS CFAR simulations are also done for comparison. Improvement factor of detectors are close to each other where GOCA CFAR has the best result. Considering the original detectors OS CFAR is the best. However, when overall results are considered improved GOCA CFAR is the best.

Simulations with Single Target are divided into two. First one is done to analyze the way the performance changes with the range of target. DPM is applied to CA CFAR, SOCA CFAR and GOCA CFAR. Moreover, OS CFAR simulations are also done for comparison also in this analysis. It has been observed that in original detectors false detections are mainly composed of ghosts. DPM is capable of eliminating them for GOCA CFAR and CA CFAR. Therefore, for these detectors very high improvement factors could be obtained. Moreover, P_D value does not reduce after DPM. However, DPM fails in improving SOCA CFAR. Very low improvement factor is obtained for this detector. OS CFAR detector achieves good P_D values at close ranges but P_{FD} value is as high as the original CA CFAR detector. As the range increases P_{FD} decreases but P_D value reduces below the tolerable values. As a result, it is observed that CA CFAR detector has a better performance compared to OS CFAR after DPM is applied.

In order to make a fair comparison, threshold scale factor α_{CA} of CA CFAR is set to a value to obtain a P_{FD} value equal to P_{FD} of CA CFAR detector after DPM is applied. Then P_D values of these two detectors are compared. P_D values of original CFAR detector are below 0.614 which are not practically acceptable. On the other

hand, P_D values of CA CFAR detector after DPM are 1 which is the highest value that can be achieved.

Second type of simulation that is done with one target analyzes the way the performance changes with the Doppler frequency of target. This analysis is done only for CA CFAR. In these analyses, Doppler frequencies do not perfectly match with Doppler bins. These frequencies correspond to the frequencies between two adjacent Doppler bins. Therefore, change in P_D at both close Doppler bin and far Doppler bin is investigated. As a result of the simulations, for almost every Doppler frequency, DPM achieves reducing P_{FD} 10^2 times. Moreover, for half of the Doppler frequencies P_{FD} is reduced 10^3 times. Therefore, it can be said that first aim of DPM is achieved which is reducing P_{FD} . However, it is not the case for the second aim of DPM which is keeping P_D of original CA CFAR. For the Doppler frequencies close to zero Doppler, P_D reduces below the acceptable values. For the Doppler frequencies close to Doppler bins, DPM is capable of keeping P_D of close Doppler bin and reducing P_D of far Doppler bin. As a result target will only show up at the Doppler bin which is close to its Doppler frequency with high probability. For the Doppler frequencies around the middle of the adjacent Doppler bin, DPM may reduce P_D of close Doppler bin while keeping P_D of far Doppler bin. In this case, far Doppler bin is chosen as the Doppler bin of the target's Doppler frequency.

In simulations with two targets, target masking behaviors are investigated. Three types of scenarios are investigated for GOCA CFAR and CA CFAR detectors. SOCA CFAR detector is not handled since it has been seen that Doppler pattern method fails in this type of detector. Moreover, OS CFAR detector is not handled because it fails at range of target's range used in simulation. In the cases where SIR values of two targets are close to each other, DPM is successful both for GOCA CFAR and SOCA CFAR. P_D values do not decrease considerably while P_{FD} values decreases dramatically. On the other hand, when SNR of two targets are

different from each other, DPM is successful for CA CFAR but it fails in GOCA CFAR. DPM achieves reducing P_{FD} but it also reduces P_D of the target with smaller SIR.

Finally, it can be said that DPM achieves its first aim which is reducing P_{FD} . However, it is capable of keeping P_D of original CFAR at Doppler frequencies close to Doppler bins. At Doppler frequencies around the middle of two adjacent Doppler bins, DPM fails in choosing the correct Doppler bins. Moreover, another result that can be extracted from improvement factors is that DPM is successful in improving CA CFAR and GOCA CFAR but not in improving SOCA CFAR.

As a future work, number of Doppler patterns may be increased to improve the performance of DPM. Doppler patterns of the frequencies that are in the middle of two adjacent Doppler bins can also be formed and used. This way, performance of DPM at Doppler frequencies around the middle of two Doppler bins can be improved.

REFERENCES

- [1] Merrill I. Skolnik, *Introduction to Radar Systems*, McGRAW-HILL, 2001.
- [2] Mark A. Richards, *Fundamentals of Radar Signal Processing*, McGRAW-HILL, 2005
- [3] Aluffi Pentini F. , Farina A., Zirilli F., *Radar Detection of Targets Located in a Coherent K-Distributed Clutter Background*, IEE Proc. 1992, pp.239-245
- [4] Conte E., Longo M., Lops M., Ullo S.L., *Radar Detection of Signals With Unknown Parameters in K-distributed Clutter*, IEE Proc. 1991, pp.131-138
- [5] Yalçın Tanık , Mete Severcan, *Radar Signal Models-2*, Aselsan Technical Report, Sep 2004
- [6] Fatih Canatan, Ülkü Doyuran, Sencer Koç, Mete Severcan, Yalçın Tanık Ali Özgür Yılmaz, *Aselsan Technical Report*, 2005
- [7] Handan Ağırman, *Waveform Design for Pulse Doppler Radar*, M.S Thesis, 2005
- [8] Mete Severcan, *MTI MTD Techniques*, Aselsan Technical Report, 2004
- [9] G.W.Stimson, *Introduction to Airborne Radar*, 2nd ed. Scitech 1998
- [10] Alan V. Oppenheim, Ronald W. Schaffer, John R. Buck, *Discrete Time Signal Processing , Prentice Hall Signal Processing Series*, 1998

- [11] Yalçın Tanık, *Simplifications for Clutter/Doppler Filters* , Aselsan Technical Report, 2005
- [12] Yalçın Tanık , *Radar Signal Models*, Aselsan Technical Report, 2003
- [13] Yalçın Tanık , *Phase Noise Effects* , Aselsan Technical Report, 2005
- [14] Curtis Schleher, *MTI and Pulsed Doppler Radar*, Artech House, 1991
- [15] Byron Edde, *Radar Principals, Technology, Applications*, Prentice Hall, 1992
- [16] Weiss, M., *A CFAR Thresholding Approach Based on Test Cell Statistics*, *Proceedings of the 2004 IEEE Radar Conference*, pp, 349-354, 2004
- [17] F. Gini, *Sub-optimum coherent radar detection in a mixture of K- distributed and Gaussian clutter*, *Proc. Inst., Inst. Elect. Eng. F*, vol. 144, no. 1, pp. 39–48, Feb. 1997.
- [18] A. Farina, F. Gini, M.V. Greco, P. Lombardo, *Coherent Radar Detection of Targets Against a Combination of K-distributed Clutter*, *Proceedings of the IEEE International RADAR Conference*, 1995
- [19] A. Farina, Gini F, M.V Greco., K.J Sangston., *Optimum and Sub-Optimum Coherent Radar Detection in Compound Gaussian Clutter, a Data-Dependent Threshold Interpretation*, *Proceedings of the IEEE National Radar Conference*, 1996
- [20] Hermann Rohling, *Radar CFAR Thresholding in Clutter and Multiple Target Situations* ,*IEEE Transactions on Aerospace and Electronics Systems* Vol. AES-19, No.4, 1983

- [21] F.E. Nathanson, *Radar Design Principles*, 2d ed. McGraw-Hill,1991
- [22] F.J. Harris, , *On the Use of Windows for Harmonic Analysis with the Discrete Fourier Transform*, Proceedings of the IEEE vol.68, no. 1, pp.51-83,1978
- [23] F. Gini, M.V. Greco, A. Farina, *Clairvoyant and Adaptive Signal Detection in Non-Gaussian Clutter: A Data-Dependent Threshold Interpretation*, IEEE Transactions on Signal Processing, Vol.7 No.6, 1999
- [24] R. De Angelis, A. Farina, F. Zirilli, *The Use of Perturbation Methods in the Problem of Radar Detection Against a K-clutter Background*, IEE Proc., pp. 243-251
- [25] Yalçın Tanık, *Phase Noise Models*, Aselsan Technical Report, 2005
- [26] J. B. Billingsley, *Low Angle Radar Land Clutter Measurements and Empirical Models*, Lincoln Laboratory MIT, William Andrew Publishing, 2002
- [27] Sencer Koç, *Radar Simulator*, in Aselsan Technical Report, November 2005